THE
PHYSICAL REVIEW

A journal of experimental and theoretical physics established by E. L. Nichols in 1893

SECOND SERIES, VOL. 102, NO. 6 JUNE 15, 1956

Spectral and Angular Distribution of Ultraviolet Radiation from the 300-Mev Cornell Synchrotron*

D. H. TOMBOULIAN AND P. L. HARTMAN
Department of Physics, Cornell University, Ithaca, New York
(Received November 22, 1955)

The spectral characteristics of the radiation emitted by high-energy centripetally accelerated electrons have been examined for various electron energies over a wide wavelength range extending down to 60 A. Following preliminary remarks concerning the source and spectral distribution laws deduced from theory, the paper describes an experimental investigation of the spectrum. The spectrum is examined in the quartz region but the major portion of the work deals with measurements in the soft x-ray region where a grazing incidence vacuum spectrograph is used to record the average power spectrum emitted over a partial or full synchrotron acceleration interval during which the electron energy reaches the values of 233 Mev or 321 Mev, respectively. In each case the radiation is detected photographically and photometric procedures are followed in reducing the spectrograms. The method of reduction takes into account aspects of the actual source, and a variety of instrumental factors dealing with the dispersion, the transmission, the spectral response, and also the geometrical effects of the optical system involved. The calibration of the emulsion is carried out according to schemes appropriate to each wavelength region. While heterochromatic photometry can be employed in the quartz region, in the vacuum region the emulsion response is taken as constant for fixed energy independent of wavelength. The wavelength dependence of the grating reflecting power is determined by calculations based on measurements with nearly monochromatic sources. This information makes it possible to reduce the exposures obtained with the synchrotron continuum over the wavelength region extending from 60 A to about 200 A. At longer wavelengths the grating response is deduced by treating a portion of the 233-Mev spectrum as known; the grating efficiency obtained in this manner is then used to reduce the corresponding portion of the 321-Mev exposure.

The results on the spectral distributions are in reasonably good agreement with the corresponding predictions from classical radiation theory of accelerated electrons. The observed distribution in the spatial spread of the radiation at various positions in the spectrum can also be accounted for if a plausible model is adopted for the diffuseness of the actual source in verifying the theoretical expressions for the angular distribution due to a single radiator. It is pointed out that such continuous radiation may serve as a suitable source for making absorption measurements in the far ultraviolet. The absorption spectra of metallic Be and Al are obtained by the use of the continuum. The Be-K and Al-$L_{2,3}$ discontinuities, occurring at 111 A and 170 A, respectively, are clearly visible in two orders. It is also suggested that the source may possibly be utilized as a standard for the purpose of calibrating detectors in the ultraviolet region.

A. INTRODUCTION

IT is well known that high-energy electrons subject to centripetal acceleration emit electromagnetic radiation whose spectral distribution varies markedly with the electron energy. That such electrons are effective radiators is not surprising when one considers that the magnitude of the acceleration is about $10^{16}g$ when the particle velocity nears c in an orbit of 1-meter radius.

In 1898 Lienard[1] gave a formula for the rate of radiation from a centripetally accelerated charge and in 1908 Schott[2] further developed the classical theory in connection with the study of atomic models. More recently, interest in the problem has been renewed with the recognition that the radiative losses incurred by the electron place a severe limitation[3] on the electron energy attainable in the operation of other than linear accelerators. A number of pertinent investigations have been reported.[4–9]

On the experimental side, studies were first conducted by a group of investigators at the General Electric

* The research was supported in part by the Office of Ordnance Research, U. S. Army.

[1] A. Lienard, L'Eclairage Elec. **16**, 5 (1898).

[2] G. A. Schott, *Electromagnetic Radiation* (Cambridge University Press, Cambridge, 1912).

[3] In the new Cornell synchrotron, for example, it will be necessary to impart to the electron about 130 kev per turn just to supply the radiative losses and maintain an electron at an equilibrium energy of 1.5 Bev in an orbit nearly 4 m in radius.

[4] D. Iwanenko and I. Pomeranchuk, Phys. Rev. **65**, 343 (1944).

[5] E. M. McMillan, Phys. Rev. **68**, 144 (1945).

[6] J. P. Blewett, Phys. Rev. **69**, 87 (1946).

[7] L. I. Schiff, Rev. Sci. Instr. **17**, 6 (1946).

[8] J. Schwinger, Phys. Rev. **70**, 798 (1946).

[9] J. Schwinger, Phys. Rev. **75**, 1912 (1949).

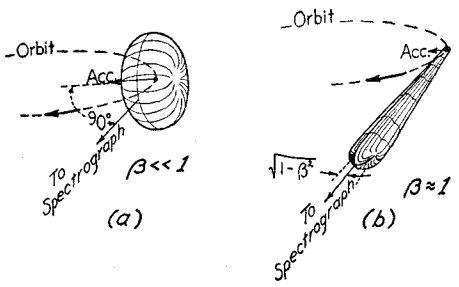

FIG. 1. Qualitative radiation patterns to be expected from electrons in a circular orbit (a) at low energy and (b) as distorted by relativistic transformation at high energy. [See also discussion in W. K. H. Panofsky and M. Phillips, *Classical Electricity and Magnetism* (Addison-Wesley Press, Cambridge, 1955), pp. 301–307.]

Research Laboratories. They reported[10] on the visible radiation in 1947 in connection with the operation of the 70-Mev General Electric synchrotron and later carried out an investigation[11] on the spectral distribution of the radiation in the visible part of the spectrum. Their results were in agreement with the spectral distribution formulas based on an extensive classical treatment of the problem by Schwinger.

With the availability at Cornell of a 300-Mev synchrotron and suitable spectroscopic equipment, the idea of investigating the characteristics of the radiation in the extreme ultraviolet appeared attractive for several reasons. First was the natural interest in observing the radiation in its heretofore unexplored region of much shorter wavelengths. Secondly, there were utilitarian motives. It was felt that the synchrotron radiation could serve as an intense source of continuous radiation for solid-state spectroscopy, particularly since a suitable source is lacking in making absorption measurements. There was also the possibility of treating the source as a standard in the soft x-ray region and utilizing it for the purpose of calibrating various detectors in terms of the known intensity distribution. While the experiment was under consideration, some doubt was cast on the validity of the classical treatment when it was indicated[12] that considerable deviation from the results of classical theory were to be expected even at the relatively low electron energies of 200 Mev. Although subsequent calculations[13–16] showed this expectation to be in error, there was no experimental evidence, and a verification by actual observation of the spectrum was an additional inducement at the time. Corson[17] has since carried out measurements on the total energy loss of electrons in the Cornell synchrotron and has demonstrated that independently of the spectral distribution, the classical expression for the total rate of radiation appears to predict satisfactorily the experimentally observed loss.

This paper presents the results of the investigation which to date have been reported only in a preliminary manner.[18–20]

B. CHARACTERISTICS OF THE RADIATION

I. Descriptive Remarks

On sighting along a tangent to the circular electron orbit in a high-energy device by way of a mirror, the observer sees an intense blue-white glow. In high-energy and high electron-density machines, the light intensity may be so great as to illuminate a wall, opposite the exit port, in daylight. If the line of observation is shifted from the plane of the orbit, there is a rapid drop in intensity, and a change in the quality suggesting a slight predominance of longer wavelengths. The light is linearly polarized, with the electric vector parallel to the plane of the orbit. While the radiation is highly directional, the wave fronts nonetheless are spherical about the source, as attested by focusing tests with camera or theodolite.

Some fairly simple arguments can be presented concerning the origin and frequency limits of the radiation.[9,15] The electron is of course radially accelerated, but the usual low-velocity toroidal radiation pattern with its zero at an angle of 90° to the directions of maxima, as in Fig. 1(a), is greatly distorted by virtue of the relativistic effects calculated from the Lorentz transformation. In particular, the zeros of the radiation pattern are now located in the orbital plane at angles $\theta=(1-\beta^2)^{\frac{1}{2}}$ from the direction of motion (which is also that of the radiation maximum) as indicated schematically in Fig. 1(b). In the diagram, the angle $(1-\beta^2)^{\frac{1}{2}}=m_0c^2/E$ is the transformed angle of 90°. In the case of such a narrow cone (actually, as indicated, it is neither quite conical in shape nor symmetrical about $\theta=0°$), the radiation which reaches an observer is emitted only from a very small portion of the orbit having angular extent of about $2(1-\beta^2)^{\frac{1}{2}}$. The time during which such radiation is emitted is given by $2R(1-\beta^2)^{\frac{1}{2}}/c$, where R is the radius of the orbit. Since the source is approaching the observer with a velocity almost equal to c, this pulse is greatly compressed by a factor of $(1-\beta^2)$. Hence the duration of the pulse at the observer is of the order of $R(1-\beta^2)^{\frac{3}{2}}/c$, equal to $(R/c)(m_0c^2/E)^3$ in terms of the rest energy m_0c^2 and the actual energy E of the electron. Consequently, the Fourier spectrum of the pulse at the observer will contain frequencies whose approximate upper limit has a

[10] Elder, Gurewitsch, Langmuir, and Pollock, Phys. Rev. **71**, 829 (1947).
[11] Elder, Langmuir, and Pollock, Phys. Rev. **74**, 52 (1948).
[12] G. Parzen, Phys. Rev. **84**, 235 (1951).
[13] Judd, Lepore, Ruderman, and Wolff, Phys. Rev. **86**, 123 (1952).
[14] H. Olsen and H. Wergeland, Phys. Rev. **86**, 123 (1952).
[15] L. I. Schiff, Am. J. Phys. **20**, 474 (1952).
[16] M. Neuman, Phys. Rev. **90**, 682 (1953).
[17] D. R. Corson, Phys. Rev. **90**, 748 (1953).
[18] P. L. Hartman and D. H. Tomboulian, Phys. Rev. **87**, 233(A) (1952).
[19] P. L. Hartman and D. H. Tomboulian, Phys. Rev. **91**, 1577 (1953).
[20] D. H. Tomboulian and P. L. Hartman, Phys. Rev. **95**, 600(A) (1954).

magnitude equal to the reciprocal of the duration of the pulse. There will also be higher frequency components whose strength diminishes with frequency. For an electron moving in a circular orbit the pulse is repeated at the orbital angular frequency ω_0, as determined by the accelerator. In principle, therefore, the harmonics will be integral multiples of ω_0 and the spectrum will contain a discrete set of frequencies which extend from the peak values down to the lowest frequency ω_0.

Feynman has suggested a different approach,[21] according to which the radiation observed from any source is to be described in terms of the acceleration of a projection of the source. The latter is to be projected on to a plane normal to the direction of observation, the projection being made in retarded time. He has given a geometrical construction of this which shows clearly that in the projection plane, there result extremely high accelerations when the source approaches the observer with a velocity nearly equal to c. The orbit is to be regarded as pulled away from the observer at the rate c. The motion of the electron in its orbit thus appears stretched out into an epicycloidal curve whose cusps get sharper and sharper, the closer the actual orbital velocity of the electron approaches the value of c. This space curve is then to be imagined as pulled through the observer's projection plane at the rate c, the acceleration of the point where the curve intersects the plane being taken as a measure of the electromagnetic field observed from the actual electron in its orbit. Very high frequencies will thus result from the cusps. Also, if the projection plane is not normal to the orbital plane, the cusps become less sharp and there is a degradation in frequency. This corresponds to the case of an observer who receives the radiation along directions slightly inclined to the orbital plane.

II. Expressions for Various Spectral Distributions

1. The Monoenergetic Spectral Distribution

The most complete treatment of the radiation problem is that given by Schwinger.[9] Since a clear distinction must be drawn between quantities observed in practice and those calculated for the motion of a single electron in a circular orbit, we shall now include several pertinent conclusions taken from Schwinger's formulation, with particular emphasis on the spectral and angular distribution of monoenergetic electrons and of electrons accelerated sinusoidally to a certain peak energy.

Schwinger has derived a general expression [Eq. (I.33) in reference 9] for the instantaneous power radiated into a unit solid angle in a given direction per unit frequency interval centered about a given frequency. A special result for the total energy loss ΔE per revolution of an electron in a circular orbit of radius R may be deduced from his general expression and assumes the form

$$\Delta E_{\text{kev}}=88.5(E_{\text{Bev}})^4/R_{\text{meters}}, \tag{1}$$

where E is the energy of the electron. This expression checks the results of simpler calculation. When integrated over all angles, the general expression yields the formula

$$P(\omega,t)=\frac{3^{\frac{3}{2}}}{4\pi}\left(\frac{e^2}{R}\right)\left(\frac{E}{m_0c^2}\right)^4\frac{\omega_0\omega}{\omega_c^2}\int_{\omega/\omega_c}^{\infty}K_{5/3}(\eta)d\eta \tag{2}$$

for the instantaneous power flow into all angles per unit frequency interval centered about the radiated frequency ω. In (2), ω_c is the so-called critical angular frequency parameter and is defined by the relation

$$\omega_c=\tfrac{3}{2}\omega_0(E/m_0c^2)^3, \tag{3}$$

where ω_0 is the orbital angular frequency ($\omega_0=c/R$). The parameter ω_c represents a frequency which is close to the frequency corresponding to the peak of the spectral distribution but falling somewhat short of it. The integrand in (2) involves Bessel functions of imaginary argument and fractional order, as may be seen from

$$K_{5/3}(\eta)=\frac{\pi}{\sqrt{3}}\left\{\frac{4}{3\eta}[i^{2/3}J_{-2/3}(i\eta)-i^{-2/3}J_{2/3}(i\eta)]+[i^{1/3}J_{-1/3}(i\eta)-i^{-1/3}J_{1/3}(i\eta)]\right\}. \tag{4}$$

In the experimental study of spectral distributions, it is the wavelength rather than the frequency which is involved in the measurements. In terms of this variable, Eq. (2) reduces to

$$P(\lambda,t)=\frac{3^{5/2}}{16\pi^2}\left(\frac{e^2c}{R^3}\right)\left(\frac{E}{m_0c^2}\right)^7G(y), \tag{5}$$

giving us an expression for the instantaneous power per unit wavelength interval about the wavelength λ. The function $G(y)$ appearing in (5) is given by

$$G(y)=y^3\int_y^{\infty}K_{5/3}(\eta)d\eta, \tag{6}$$

where

$$y=\lambda_c/\lambda, \quad \lambda_c=(4\pi R/3)(m_0c^2/E)^3. \tag{7}$$

In passing, we note that for the old Cornell synchrotron used in the present experiments, the wavelength λ_c which roughly marks the termination of the spectrum, could be calculated from

$$\lambda_c=(55.9\times10^8)/E_{\text{Mev}}{}^3, \text{ (in Angstroms)} \tag{8}$$

since the radius of the accelerator was very nearly equal to 1 m.

The expression for $G(y)$ given by Eq. (6) serves as a sort of universal spectral distribution curve which once plotted can be used to obtain the actual distribution at any energy E. From the tabulated values[22] of the contents of $K_{5/3}(\eta)$ given in (4), the integral can be evaluated numerically, resulting in a function of y which when multiplied by y^3 yields $G(y)$. For a

[21] R. P. Feynman (private communication).

[22] E. Jahnke and F. Emde, *Tables of Functions* (Dover Publications, New York, 1945).

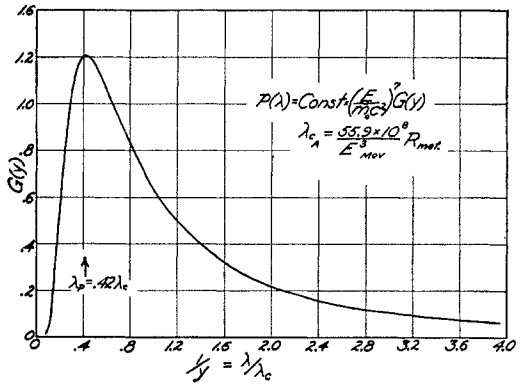

FIG. 2. Universal spectral distribution curve for the radiation from monoenergetic electrons. $P(\lambda)$ is the instantaneous power radiated per angstrom.

given value E, the numerical value of $P(\lambda)$ at any λ may be obtained by first calculating λ_c from (8) and then converting λ into y. This determines $G(y)$. The absolute value of $P(\lambda)$ is obtained on multiplying the appropriate value of $G(y)$ by the constant factor appearing in (5). This gives the desired spectral distribution for the particular energy E.

A plot of $G(y)$ is shown in Fig. 2. With the aid of this curve one can see that the distribution rises sharply with energy. Consider, for instance, the magnitude of $P(\lambda)$ near the peak as specified by $\lambda=\lambda_c$ or $1/y=1$. Then, as the energy increases, the value of $P(\lambda)$ defined by λ_c rises as E^7 as can be seen from relation (5), while the wavelength position λ_c shifts towards shorter values as E^{-3} in accordance with (7). As a second feature of interest, we note that the spread in wavelength between half-power points can also be obtained from the universal curve. The power per angstrom drops much more rapidly on the short-wavelength side of λ_p, the wavelength corresponding to the peak of the distribution. The peak itself occurs at a wavelength which is considerably shorter than the parameter λ_c. The relation between them as deduced from the plot of $G(y)$ is $\lambda_p=0.42\lambda_c$. Furthermore, if λ_2 and λ_1 are the wavelengths corresponding to the half-power ordinates, one sees that $(\lambda_p-\lambda_1)=0.20\lambda_c$ and $(\lambda_2-\lambda_p)=0.64\lambda_c$, so that the width of the distribution at half-maximum is $0.84\lambda_c$. A family of monoenergetic distribution curves included in Fig. 3 illustrates how markedly the distribution changes with energy.

2. *Average Power Spectrum*

The same type of numerical calculation may be employed in deducing the average power spectrum emitted by electrons accelerated to a maximum energy E_m under the assumption that the instantaneous energy E_t varies with the time t in accordance with

$$E_t=E_m\sin(\pi t/2T), \tag{9}$$

in which $4T$ represents the period of the sinusoidal magnetic field.

The time variation of the magnetic field is very nearly sinusoidal except at the beginning of the cycle. To a high degree of approximation the energy is proportional to the magnetic field. Strictly speaking, because of the radiative losses, the energy does not increase quite in proportion to the field but the departure is small.[23]

The acceleration interval may be made equal to T, or to a smaller value T'. In the latter case, the electron energy is allowed to increase sinusoidally up to a value E' which is less than E_m. In the case of the full $\frac{1}{4}$-cycle acceleration, the average power spectrum is given by

$$\bar{P}_{\text{full}}(\omega)=\frac{1}{T}\int_0^T P(\omega,t)dt. \tag{10}$$

The integration in Eq. (10) can be carried out by the introduction of a variable τ, defined by

$$\tau=\frac{\lambda_c(t)}{\lambda_m}=\left(\frac{E_m}{E(t)}\right)^3=\left(\sin\frac{\pi t}{2T}\right)^{-3}, \tag{11}$$

where

$$\lambda_c(t)=\frac{4\pi R}{3}\left(\frac{m_0c^2}{E(t)}\right)^3. \tag{12}$$

In terms of the wavelength, the result is expressible as

$$\bar{P}_{\text{full}}(\lambda)=\frac{3^{5/2}}{16\pi^2}\left(\frac{e^2c}{R^3}\right)\left(\frac{2}{3\pi}\right)\left(\frac{4\pi R}{3}\right)^3\left(\frac{m_0c^2}{E_m}\right)^2\frac{1}{\lambda^3}$$
$$\times\int_1^\infty \tau^{-1/3}(\tau^{2/3}-1)^{-1/2}d\tau\int_{(\lambda_m/\lambda)\tau}^\infty K_{5/3}(\eta)d\eta, \tag{13}$$

in which λ_m appearing in the lower limit of the last integral is equal to

$$\lambda_m=\frac{4\pi R}{3}\left(\frac{m_0c^2}{E_m}\right)^3. \tag{14}$$

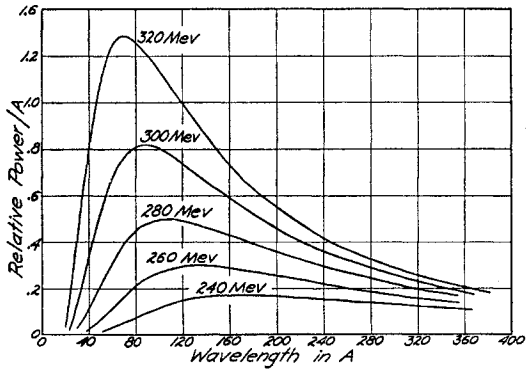

FIG. 3. Comparison of the relative spectral distributions for the radiation from monoenergetic electrons at various energies. This illustrates the sensitive variation of the distribution with energy.

[23] J. Schwinger, "On Radiation by Electrons in a Betatron," 1945. This unpublished manuscript was made available to the authors by courtesy of the Office of Naval Research.

Introducing the dimensionless quantity $x=\lambda_m/\lambda$, Eq. (13) may be put into the form

$$\bar{P}_{\text{full}}(\lambda)=\frac{3^{5/2}}{8\pi^3}\left(\frac{e^2c}{R^3}\right)\left(\frac{E_m}{m_0c^2}\right)^7[x^4G(x)] \qquad (15)$$

with

$$G(x)=\int_1^\infty (\tau^{2/3}-1)^{1/2}K_{5/3}(x\tau)d\tau. \qquad (16)$$

As in the case of monoenergetic electrons, a universal curve for the full $\frac{1}{4}$-cycle distribution may be obtained by plotting $[x^4G(x)]$, as in Fig. 4. The actual average power spectrum for any peak energy E_m can then be found by the use of Eq. (15). It is of interest to note that the same result may also be obtained graphically from the summation of a series of monoenergetic curves (see Fig. 3), the individual distributions being weighted according to the relative times spent over a given energy interval at the particular energies involved. Indeed, this method was employed to provide a check on the results of numerical calculations involved in evaluating the integrals in Eq. (13). As before, one may obtain the half-width and the wavelength corresponding to the peak of the average power spectrum from the graph in Fig. 4. These are found to be $1.00\lambda_m$ and $0.5\lambda_m$, respectively.

The determination of the average power spectrum curves in the case of part $\frac{1}{4}$-cycle acceleration is carried out along similar lines. In this instance the accelerating rf voltage is turned off at the time T', before the time T at which the sinusoidally varying magnetic field passes through its maximum. The electron energy thus rises only to E' rather than to E_m. The average power spectrum is now defined by

$$\bar{P}_{\text{part}}(\lambda)=\frac{1}{T'}\int_0^{T'} P(\lambda,t)dt, \qquad (17)$$

which reduces to

$$\bar{P}_{\text{part}}(\lambda)=\frac{3^{3/2}}{8\pi^3}\left(\frac{e^2c}{R^3}\right)\left(\frac{T}{T'}\right)\left(\frac{E_m}{m_0c^2}\right)^7 x^3I(x,\tau'), \qquad (18)$$

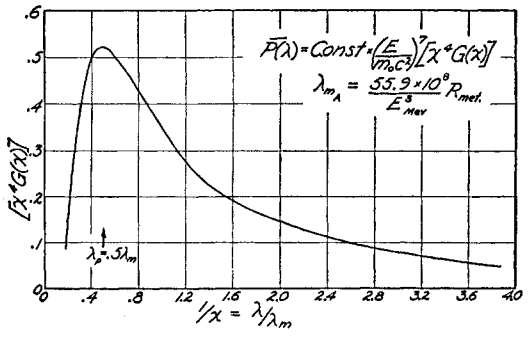

FIG. 4. Universal spectral distribution curve for the radiation from electrons with energy increasing sinusoidally over a full quarter cycle. $\bar{P}(\lambda)$ is the average power radiated per angstrom.

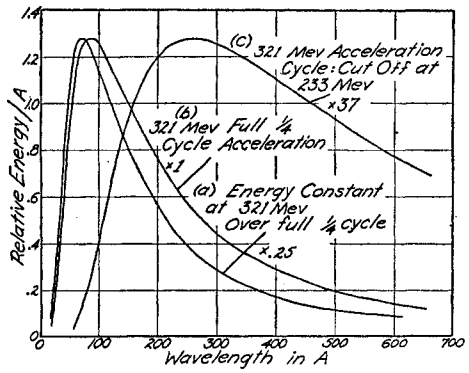

FIG. 5. Comparison between the spectral distributions (a) from monoenergetic electrons radiating over the full $\frac{1}{4}$-cycle, (b) from electrons (of sinusoidally increasing energy) which attain the energy of 321 Mev at the peak of the cycle, and (c) from electrons accelerated only to 233 Mev over part of the $\frac{1}{4}$-cycle 321-Mev interval.

where $x=\lambda_m/\lambda$, [λ_m is given by Eq. (14)], and

$$I(x,\tau')=\int_{\tau'}^\infty \tau^{-1/3}(\tau^{2/3}-1)^{-1/2}d\tau\int_{x\tau}^\infty K_{5/3}(\eta)d\eta, \qquad (19)$$

with

$$\tau'=\left(\sin\frac{\pi T'}{2T}\right)^{-3}=\left(\frac{E_m}{E'}\right)^3. \qquad (20)$$

The result of the numerical integration of (18), again checked by graphical summation of weighted monoenergetic curves, is shown in Fig. 5 for $E'=233$ Mev and $E_m=321$ Mev. For the sake of comparison, two other curves are also included. These show the spectral distributions for a monoenergetic electron at 321 Mev and for an electron which attains the peak energy of 321 Mev during full $\frac{1}{4}$-cycle acceleration, both radiating for the same period of time.

3. *Angular Distributions*

Formulas which describe the angular distribution of the radiation are also included in the work of Schwinger,[9] who gives an expression for $P(\psi,\omega,t)$, the power emitted per unit angle relative to the orbital plane, and per unit angular frequency at the time t. By the use of this general distribution function, in which the angle ψ is defined as the angle between the direction of emission and the orbital plane, it may be demonstrated that the half-angle which contains the major portion of the radiation is m_0c^2/E as cited earlier. In terms of the wavelength λ, the corresponding angular distribution is given by

$$P(\psi,\lambda,t)=\frac{3}{4\pi^2}\frac{e^2}{R}\left(\frac{\lambda_c}{\lambda}\right)^2\left(\frac{2\pi c}{\lambda^2}\right)\left(\frac{E}{m_0c^2}\right)^2\left[1+\left(\frac{E\psi}{m_0c^2}\right)^2\right]^2$$
$$\times\left[K_{2/3}^2(\xi)+\frac{(E\psi/m_0c^2)^2}{1+(E\psi/m_0c^2)^2}K_{1/3}^2(\xi)\right], \qquad (21)$$

and represents the instantaneous power per unit angle

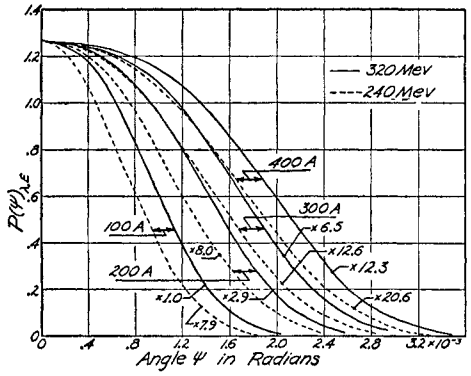

FIG. 6. Curves which show the behavior of the distribution in angle ψ referred to the orbital plane at four different wavelengths and two energies. The curves are all normalized to the same peak value at $\psi=0$ by the factors indicated. $P(\psi)|_{\lambda,E}$, represents (in arbitrary units) the instantaneous power radiated per angstrom at the wavelength λ per unit angle relative to the orbital plane at the angle ψ relative to the orbital plane.

at the angle ψ and per unit wavelength centered at λ. In Eq. (21),

$$\xi=\frac{\lambda_c}{2\lambda}\left[1+\left(\frac{E\psi}{m_0c^2}\right)^2\right]^{3/2}. \tag{22}$$

The behavior of the general distribution function $P(\psi,\lambda,l)$ was studied graphically in the manner here described: Holding E and λ constant, the partial distribution $P(\psi)|_{E,\lambda}$ was obtained from Eq. (21) by assigning values to the angle ψ. [Actually it was more convenient to take a fixed set of values for ξ lying in the range 0 to 4 and from Eq. (22) to determine the angle ψ corresponding to the chosen values of ξ. The set of values selected for ξ could also be used in evaluating one set of quantities specified by the functions $K_{2/3}{}^2(\xi)$ and $K_{1/3}{}^2(\xi)$.] Then, keeping λ fixed, the above process was repeated for a set of values for the energy E, spaced 20 Mev apart, and ranging from $E=320$ Mev down to $E=180$ Mev. The energy dependence on time was taken to be sinusoidal and the vertical spread (distribution in ψ) was calculated at the fixed wavelength by summing up the appropriately weighted monoenergetic distributions for all energies up to 240 Mev or 320 Mev corresponding approximately to the cases of part or full $\frac{1}{4}$-cycle acceleration. Such summations over the energy were carried out for $\lambda=100$, 200, 300, and 400 A. A plot of a family of curves representing $P(\psi)|_{E,\lambda}$ is to be found in Fig. 6. For the purpose of comparison, the monoenergetic distributions at the four wavelengths are normalized to the same arbitrary value. It is seen that at a fixed energy the angular spread is wider at the longer wavelengths. Though the peak value of the individual distributions changes rapidly with the energy, the energy dependence of the angular spread, at a given wavelength, is not large. At each wavelength the spread is narrower in the family of curves at the lower energy. This implies that, to get the appropriate acceleration for the projected electron in Feynman's description mentioned previously, one has to be closer to the orbital plane in the case of low-energy electrons.

The integration of $P(\psi,\omega,t)$ over all frequencies has been carried out by Schwinger who obtains the angular distribution

$$P(\psi,t)=\omega_0\frac{e^2}{R}\left(\frac{E}{m_0c^2}\right)^5\left[1+\left(\frac{E\psi}{m_0c^2}\right)^2\right]^{-5/2}\times\left[\frac{7}{16}+\frac{5}{16}\left\{\frac{(E\psi/m_0c^2)^2}{1+(E\psi/m_0c^2)^2}\right\}\right], \tag{23}$$

which is independent of frequency. Plots of this function are shown in Fig. 7 for two values of the energy parameter E equal to 321 Mev and 233 Mev, respectively. The curves, which were normalized at the peak, show that the angular spread at $E=233$ Mev is broader than that at $E=321$ Mev. In either case, the most intense radiation is seen to fall within the angle $\bar{\psi}=m_0c^2/E$. With the aid of the factor $(311/233)^5=4.95$ used to normalize the two curves to the same value, one also finds the areas under the curves, representing total energy radiated, to be in the ratio of 3.6 to 1. This is the ratio of the two energies to the fourth power as it should be according to Eq. (2).

For the sinusoidal energy variation, the numerical integration over the energy was carried out at four different wavelengths up to the peak of the cycle at 321 Mev and also to a value short of the peak at 233 Mev. The results are presented graphically in Fig. 8.

Further use will be made of these curves in connection with the experimental examination of the angular spread of the spectrum at the chosen wavelengths.

III. Aspects of the Actual Source

In attempting to verify the predictions with regard to the various spectral and angular distributions outlined in the preceding section or in contemplating the

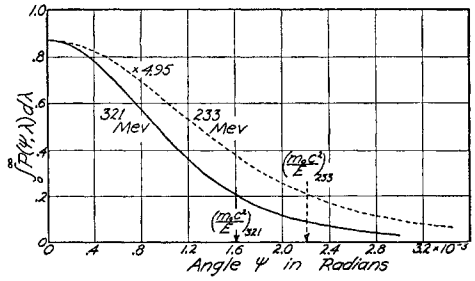

FIG. 7. Curves showing the angular distribution (for a point source) of the total radiation (summed over all wavelengths) at 321 Mev and 233 Mev. The curve at the lower energy has been multiplied by $(321/233)^5$ to normalize it to the 321-Mev distribution at the peak of the latter distribution. $\int_0^\infty P(\psi,\lambda)d\lambda$, expressed in arbitrary units, represents the instantaneous power radiated at all wavelengths per unit angle at the angle ψ relative to the orbital plane. At each energy, the value of ψ defined by (m_0c^2/E) specifies the angle within which most of the radiated energy is included.

use of the radiation in standardizing procedures, it must be realized that the emitting source consists of a "pulse" of electrons which travel together distributed in space over a portion of the orbit. It is quite likely that the motions of various electrons in the group are subject to fluctuations. A variation in the orbital radius may arise from azimuthal inhomogeneities of the magnetic field or radial oscillations. Or again, the direction of electron velocities within the group may not be parallel to a given orbital plane because of vertical oscillations.

In the course of these experiments the apparent diffuseness of the beam was brought out by two observations. First, the size of the visible glow made it clear that the radiators were smeared out in space. Secondly, the photographic recording of the far-ultraviolet spectrum showed that the intensity diminution in a direction normal to the Rowland plane[24] was more gradual than that predicted for a source consisting of a highly concentrated group of electrons.

It is not possible to state from a visual observation whether the electron beam itself is diffuse, or whether the beam which is narrow merely oscillates about a mean orbital position. (In this case the direction of the axis of the radiated cone varies slightly with position in the smear.) In attempting to interpret the observed angular spread of the radiation, it was assumed that the beam was broad but the individual orbits themselves were sharply defined.

Questions dealing with the coherence of the radiation have been investigated by Schiff,[7] McMillan,[5] and Schwinger.[23] The conclusions indicate that in any resonance accelerator a certain amount of coherent radiation is present in addition to the incoherent radiation due to individual electrons. The coherent radiation is expected to increase with decreasing bunch size but is independent of the energy. Furthermore, its spectrum lies primarily at long wavelengths, i.e., in the ultrahigh radio-frequency and microwave regions. However, due to fluctuations from a uniform distribution, each electron also radiates independently, and in the region of optical and soft x-ray frequencies the power emitted by the N electrons within the group is N times that radiated by a single electron.

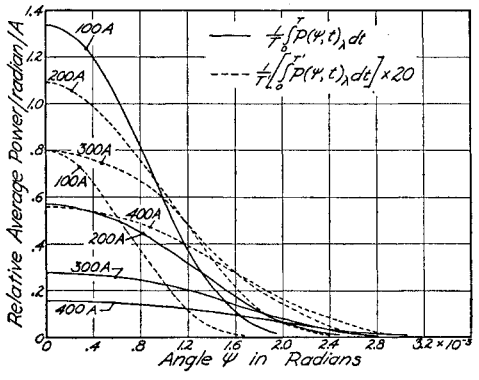

FIG. 8. Curves showing the angular distribution at various wavelengths for an electron whose energy is sinusoidally increased to a peak value of 321 Mev (———) and for one whose energy is similarly increased only to 233 Mev (– – – – –). The latter distributions have been increased by the factor 20 for ease in comparison. The ordinates represent the average power per angstrom radiated over the appropriate time interval at the wavelength λ per unit angle at the angle ψ relative to the orbital plane.

[24] Plane determined by normal to grating and line joining the midpoints of slit and grating.

C. MEASUREMENT OF THE RADIATION

In carrying out measurements on the various aspects of the spectrum, it is necessary to disperse the radiation and then detect it by radiometric, photographic, or other means. The analysis of the record requires a knowledge of the characteristics of the particular spectrograph and the detecting scheme used for the purpose. These include such factors as: (1) the fixing of the wavelength scale, (2) the instrumental dispersion, (3) the transmission or the spectral response of the optical system, (4) effects associated with the use of finite slitwidths, and those which arise from the variation of image size with wavelength, (5) the calibration and the spectral response of the detecting device. The latter may measure the average power (thermopile), may record the energy (photographic emulsion) or may count photons (photocell, counter).

To illustrate just what is involved in making relative intensity measurements, let us consider the case where a grating instrument is used for spectral studies in the far ultraviolet. Let the radiation originate from electrons which move in a circular orbit and whose energy increases sinusoidally with the time. It is proposed to determine the shape of the spectral distribution curve which represents the average rate of radiation into all angles as a function of wavelength. The radiation enters the slit, is dispersed by the grating, and falls on the photographic plate used as the detector of radiant energy. In a wavelength region free from overlapping spectral orders, let us examine the problems associated with the recording of energy. The radiation contained in a wavelength band $d\lambda$ at wavelength λ is brought to a focus along the Rowland circle and gives rise to a photographic image of width dx at some position x determined by the dispersion. However, there is no focusing in the vertical direction, that is, at right angles to the Rowland plane (this plane as well as the orbital plane of the electrons is here taken to be horizontal throughout). Hence the height of the image, if unrestricted by instrumental stops, will correspond to the vertical spread of the radiation. This spread arises from the combined effects of the angular distribution of the radiation emitted by individual electrons in the beam along with instrumental factors which produce a variation of image height with wavelength.

Next consider the situation along the Rowland circle. From the plots given in Fig. 8 for isolated radiators, it is recognized that the angular spread of the radiation at long wavelengths is wider than that at short wavelengths. At first glance this may be taken to mean that the time of exposure to the short-wavelength cone is correspondingly less and that a correction is necessary for this difference in exposure. However, along the Rowland circle, the effect due to the angular variation of the radiation cone with wavelength is compensated

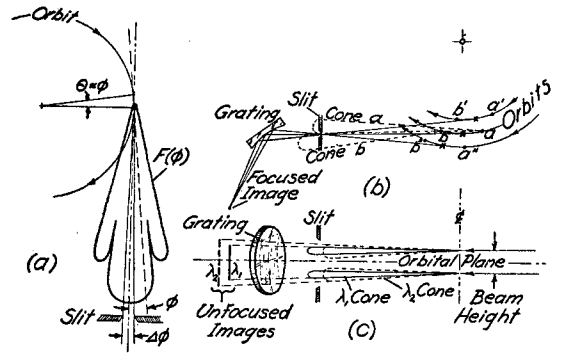

FIG. 9. Schematic representations illustrating the energy sampling. (a) Diagram which shows how $\Delta\phi$, the angular aperture of the slit, is related to the sampling of radiation having an arbitrarily shaped angular distribution $F(\phi)$. (b) Sampling in the horizontal plane looking down on the orbits and instrument. For the median orbit the sketch indicates how the energy from the extreme cones, a and b, is allowed to pass through the slit. For the three orbits shown, cones are directed centrally at the slit from the positions × which illuminate the grating at three different places as indicated. The grating, however, directs the radiation to a common focus in this projection. For the edge orbits the extreme cones into the slit come from a' and b' and from a'' and b''. (c) Sampling in the vertical plane looking edge on at the orbits (extended source). No focusing takes place in this projection, so that the image at wavelength λ_1 has a smaller height as compared to the image at the longer wavelength λ_2. This follows from the fact that at the shorter wavelength the radiation cone is narrower and the image is located closer to the slit.

for because the fixed slit accepts a proportionately larger fraction of the short wavelength cone.

Indeed, if $\Delta\phi$ is the angle subtended by the slit at the orbit, the receiving instrument collects the same fraction $\Delta\phi/2\pi$ of the total energy radiated per revolution at any wavelength λ. This may be seen by referring to the angular variables indicated in the sketch of Fig. 9(a). Assuming that we collect all the power in the vertical direction, let $F(\phi)$ represent the angular power distribution (for a particular wavelength) in the horizontal plane. Then the power radiated at the time t is

$$P(t)=\int_0^{2\pi} F(\phi)d\phi$$

and the energy radiated per turn is $(2\pi R/c)P(t)$. But the power collected by the slit of width $\Delta\phi$ is

$$\int_{\phi-\Delta\phi/2}^{\phi+\Delta\phi/2} F(\phi)d\phi \sim F(\phi)\Delta\phi$$

since $\Delta\phi$ is small[25] relative to the cone angle. In time $dt=Rd\theta/c$, the energy collected by the slit amounts to $F(\phi)\Delta\phi Rd\theta/c=F(\phi)\Delta\phi Rd\phi/c$ since ϕ sweeps across the slit by virtue of the change in θ. Thus, per turn, the energy collected is

$$\Delta\phi\int_0^{2\pi} F(\phi)Rd\theta/c=(R\Delta\phi/c)\int_0^{2\pi} F(\phi)d\phi,$$

which is just $\Delta\phi/2\pi$ times the total radiated per turn independently of the wavelength.

Owing to the spread of the electrons in the beam the actual source cannot be regarded as a point source, and we must examine how this modifies the sampling process. First let us consider only the extent of the source in the orbital plane which is taken as horizontal. Referring to Fig. 9(b), we see that the slit accepts radiation at one wavelength from an electron on the median orbit only as the electron moves from a to b. This radiation falls on the central part of the grating. Next consider a second electron whose orbit falls inside the median orbit. The slit accepts the radiation cone from this electron at a slightly different time and only while the electron is located between the points a' and b'. Similarly, for an electron in an outer orbit, the slit intercepts the cone while the electron traverses the arc $a''b''$. The radiation from these edge electrons falls on either side of the grating center. But rays which diverge from the slit in the horizontal plane are focused on the Rowland circle, so that the radiation from all the electrons is collected at the same position. Consequently no spectral displacement results from the horizontal distribution of electrons in the beam.

In the vertical direction [see Fig. 9(c)], no such focusing is present and a vertical spread of electrons in the beam results in the superposition of radiation cones displaced in a direction at right angles to the Rowland plane. The vertical cone angles are only slightly modified by the grating but, being different for different wavelengths, the actual spread of the radiation along the height of the exposure thus depends principally on the distance from the source to the Rowland circle. This point will be discussed further in connection with the study of the angular distribution of the radiation.

It follows that in the photographic record, the total grain count in an element of area having a constant width and extending the full height of the record yields a measure of the collected energy which can be associated with the radiant energy emitted by the source over the wavelength interval corresponding to the width of the strip. In practice a grain count is not feasible, but one can readily obtain a measure of the total integrated blackening within the area by crosswise scanning of the exposure with the aid of a microphotometer. It must also be remembered that, owing to the dispersion of the instrument, a given width of the exposure corresponds to a wavelength interval whose magnitude varies over the limits of the spectrum. This factor can easily be taken care of since the determination of the instrumental dispersion presents no difficulties.

Another consideration is the width of the slit. The photographed distribution is in reality a superposition of a series of displaced distributions due to elementary slits comprising the actual slit of finite width. The entrance slit will ordinarily be of negligible width. However, if it is wide, the photographed distribution may be considerably different from a narrow slit distribution. This aspect is not of importance, except in cases where there exists a rapid variation with wavelength either in the source intensity or in such instrumental characteristics as the dispersion, the grating efficiency, and the response of the emulsion. In any case, the effect can be minimized by narrowing the slit.

Even for a narrow slit, the question of image size enters into the calculations. Still considering the case of an extended source such as one emitting a discrete line spectrum, the photographic density observed in various line images will depend on the extent of the image as recorded by a particular spectrograph. Thus in a quartz instrument, the energy density in the image of a far ultraviolet line is greater than that in the larger image of a visible line of the same intrinsic intensity. For a source emitting a con-

[25] The slit width used in the grating instrument was 1.78×10^{-2} cm and the distance from source to slit was 265 cm. Hence $\Delta\phi=6.7\times10^{-5}$ radian. Calculations already presented have indicated that the radiation half-cone angle from a single electron is about 2×10^{-3} radian. Hence $\Delta\phi$ intercepts about 2% of the cone angle.

tinuous spectrum, the overlap resulting from a series of slit images eliminates the effect of image width, but a correction must be applied to include the effect of image height. Similar considerations are also valid for a grating instrument. In this instance we do not deal with the focused slit image, but rather with the superposition of astigmatic line images of slit points, and the actual height of a spectrum line again varies with wavelength.

The preceding discussion presupposes that the light originates at the slit, i.e., the source is focused achromatically on the slit and that the rays which illuminate the dispersing element are highly divergent. The situation is different in the case of the radiation from the synchrotron. Here the source may be located several meters from the slit and because of its highly directional properties the rays passing through the slit are inclined at very small angles to the Rowland plane. The earlier considerations with reference to the image width along the spectrum are still valid, but those involving the image height are somewhat different. In the case of the lens and prismatic instrument, the real source seen through the slit is imaged far forward of the instrumental focal plane. Nevertheless, in this plane, the slit is still accurately imaged as an aperture stop in the path of the incident radiation. With reference to the grazing incidence vacuum spectrograph, ordinarily there will be considerable astigmatic distortion of the image due to the large angular divergence of rays originating from a source close to the slit. However, the astigmatic effect is enormously decreased when the radiation originates from a small source placed at a large distance from the slit so that the angle between rays accepted by the slit becomes very narrow. In this optical situation simulating the case of the radiation from the synchrotron, the height of the exposure on the spectrogram will be very nearly that of the slit.

In treating the data, additional information is required concerning (1) the transmission of the prismatic instrument as a function of wavelength for the particular path traversed by the narrow pencil of rays; (2) the grating response, that is, the fraction of incident monochromatic radiation which appears in one or more spectral orders; (3) the calibration and spectral response of the detector. The determination of and the part played by these factors will be discussed in the sections which follow.

D. INVESTIGATION OF THE SPECTRUM

I. Experimental

The spectral region of chief interest in this work extended from 60 A to 450 A and was investigated by means of a grazing-incidence vacuum spectrograph. The dispersing element was a lightly ruled glass grating having 30 000 lines per inch and a radius of 154 cm. The mounting was of the Rowland type and the angle of incidence as measured from the grating surface was 4.64°, leading to a low spectrographic aperture. The dispersion varied from 0.7 A/mm at 60 A to 1.8 A/mm at 450 A. The general arrangement utilized for studying the radiation is sketched in Fig. 10. The slit housing of the spectrograph was connected through a flexible Wilson seal to the exit port in the synchrotron doughnut by sections of glass or metal tubing whose total length was about 2 m. Glass was used in the vicinity of the doughnut to avoid perturbing the ac magnetic field of the synchrotron. Between the seal in the exit port and the slit housing, a vacuum gate valve was situated containing a retractable optical quartz window which actually provided the seal. This window made it possible to determine and fix a line of sight in the direction of the visible light from the

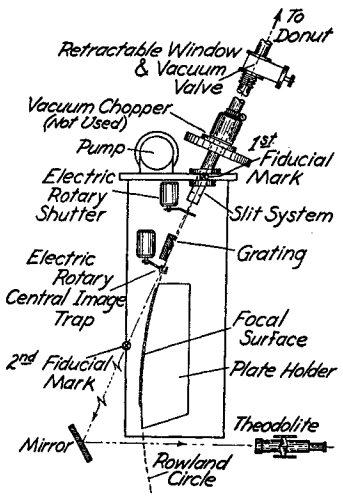

FIG. 10. Diagram which illustrates essentials of the spectrograph and aids used in alignment. The space within the rectangle is enclosed in a large retractable cylinder which serves as the evacuation chamber. The photocell used for checking the alignment is not shown. The latter was located within the spectrograph chamber back of the central image position.

machine prior to the positioning of the spectrograph. The valve served to isolate the synchrotron doughnut from the spectrograph chamber whose volume was comparable to that of the doughnut. During the initial stages in the pumping of the spectrograph the valve was kept closed until the pressure in the spectrograph and the interconnecting tube was reduced to that normally maintained in the doughnut. The valve could then be opened, connecting the two systems and allowing the radiation from points of the electron orbit to pass through the evacuated interconnecting sections directly to the slit.

A rotating disk shutter was incorporated in the tube connecting the spectrograph to the doughnut. The shutter was located directly in front of the slit, its axis intersecting the extension of the vertical line defined by the slit in order to minimize phasing errors arising from lateral shifts. Provision was made for driving the shutter through a vacuum seal at 1800 rpm in synchronism with the 30-cycle synchrotron field. By rotating the entire frame of the drive motor about its axis, the phase of the open sector in the disk could be so varied as to pass radiation over a short time interval at an arbitrarily chosen instant during the acceleration cycle. As indicated in Fig. 11, the phasing was accomplished by using a pulse derived from a permalloy peaking strip at zero magnetic field. A flash delayed by a known and variable amount served to illuminate a fiducial mark on the rotating sector shaft. By fixing the phase of the shutter in the above manner, it was possible to admit the radiation from electrons whose energies were limited to a band centered at a specified value of the energy, depending on the angular position of the motor. In the interest of avoiding complications which might have jeopardized the initial experiments in the far ultraviolet, the shutter was not (and thus far has not been) put into operation for the purpose of investigating the spectrum of sensibly monoenergetic electrons in this wavelength region. However, several exposures were made with it in a preliminary explora-

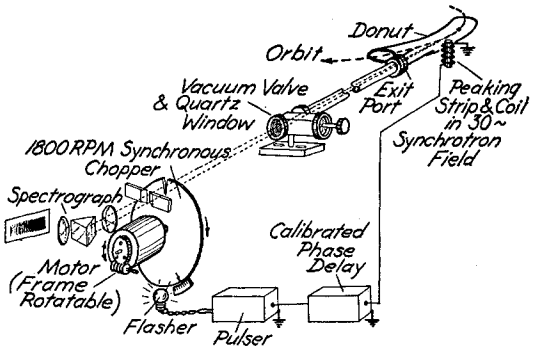

FIG. 11. Diagram showing the arrangement to be used for recording the radiation from essentially monoenergetic electrons. For work in the vacuum ultraviolet the rotating disk is enclosed, the drive shaft coming through a vacuum seal. So far the disk has not been used in the investigation of the far-ultraviolet spectrum. However, the plate of Fig. 12 was obtained with this arrangement and the quartz optical system indicated here.

tion carried out in the near ultraviolet by the use of a small quartz instrument which received the radiation transmitted by the quartz window situated in the closed vacuum valve. The disk was provided with a 3° open sector. (The opening was not designed for use at low energies. At 100 Mev the energy spread amounted to about 14 Mev, for the case where the peak energy attained during the full acceleration cycle was 300 Mev.) A set of exposures obtained with the aid of the shutter is reproduced in Fig. 12. The electron energies involved ranged from 60 Mev to 110 Mev.

The ray-like nature of the emitted radiation and low spectrographic aperture of the vacuum instrument demanded that great care be exercised in its optical alignment. Ideally, the spectrograph axis (line joining the midpoints of slit and grating) should be made coincident with the axis of the radiation cone. This requires that the Rowland plane (plane defined by the instrumental axis and the grating normal) lie in the orbital plane and that in this plane the spectrograph axis be tangent to the orbit. After leveling (the orbital plane being accurately level) and adjusting the height of the instrument (to the orbit height above reference base), the alignment procedure was carried out in the following manner: with the spectrograph out of the way and the quartz window in position in the vacuum valve, a tall mirror, adjustable in tilt and azimuth, was placed opposite the quartz window at a distance of about 15 ft. The image of the visible spot of light originating at some point on the orbit of the operating synchrotron was reflected by the mirror and observed through a theodolite with horizontal axis in the orbital plane. This procedure made it possible to establish the axial direction of the radiation in space. Leaving the mirror and theodolite position undisturbed about its vertical axis, the spectrograph was slid into position and its axis brought into coincidence with the previously fixed direction of the visible beam. The straightforward adjusting of the height and level of the Rowland plane with respect to the orbital plane having been done, there remained the careful alignment in azimuthal angle within the plane. This last adjustment was made by sighting through the theodolite and mirror at two fiducial marks previously fixed in the body of the spectrograph so as to define its axis. (These were not in the Rowland plane and therefore the theodolite had to be swung about its horizontal axis but since the latter was in the orbital plane no error was introduced.) The alignment was further verified by the use of a slit placed before a photocell so located within the spectrograph as to record the intensity of the central image. To illuminate the cell, the occultor which normally served as a trap for the central image, was moved out of the way by means of a rotary solenoid. For optimum adjustment, the cell current response to the synchrotron radiation was maximized by means of small lateral displacement of the supporting frame. Care was exercised to preserve the final position during loading and unloading of the photographic plates.

Exposures were controlled by means of a shutter placed behind the slit system and operated by the rotatory solenoid. The slit located on the Rowland circle had a width of 7 mils (1.78×10^{-2} cm). Because of their suitability for photometric work, Ilford *Q*1 plates were used in photographing the spectrum. It was not convenient to superpose a comparison spectrum, so the wavelength scale was established either by exposing the central image for a short time or by positioning the plate against a previously fixed index whose wavelength location was known. Under the particular operating conditions of the accelerator, 30-minute exposures resulted in satisfactory photographic densities for peak electron energies of about 300 Mev at only moderate electron beam intensities (about 10^9 electrons per pulse).

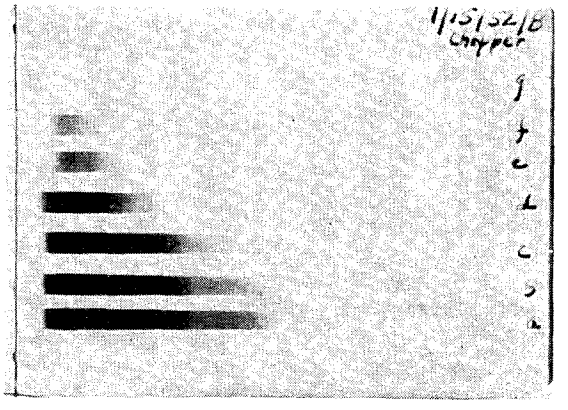

FIG. 12. Reproduction of a plate obtained with the arrangement of Fig. 11, showing spectra of the continuous radiation emitted by essentially monoenergetic electrons. The various exposures correspond to electron energies ranging from 60 Mev at the top to 110 Mev at the bottom. An exposure at 50 Mev is not visible in the reproduction. The exposures were adjusted so that, in each case, approximately the same total number of radiating electrons was involved.

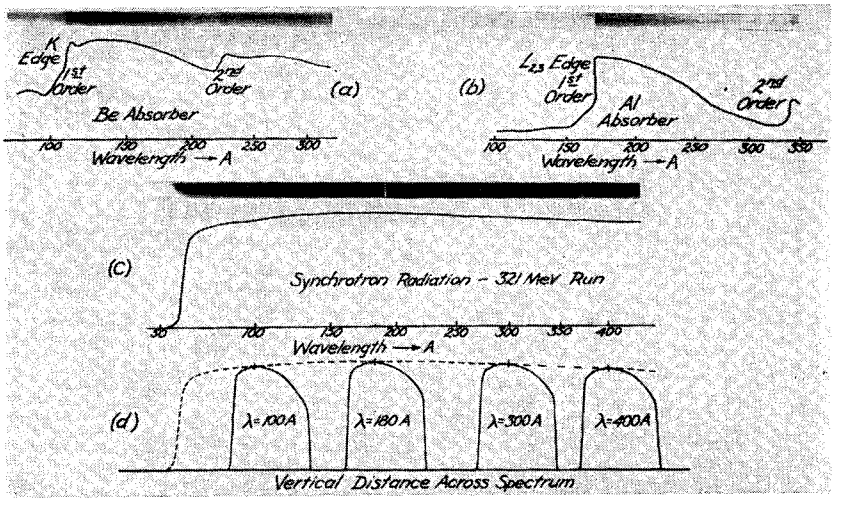

FIG. 13. Reproductions of the plates and microphotometer traces for three vacuum-ultraviolet spectra obtained by the use of the radiation from electrons whose energy was increased sinusoidally to a peak value of 321 Mev. (a) Radiation filtered through a thin Be film showing the K absorption edge which appears in the first and second order at 110 and 220 A, respectively. (b) Same radiation filtered through a thin Al film showing the $L_{2,3}$ edge in first and second order at 170 and 340 A, respectively. (c) The unfiltered synchrotron radiation. Due to the nature of the grating response and the presence of overlapping second-order radiation, the microphotometer trace of the exposure is surprisingly flat down to the abrupt cutoff at the short-wavelength region near 60 A. The tapered appearance in this region is related to the angular distribution. (d) Microphotometer records run crosswise to the exposure shown in (c) at four different wavelength positions. The traces show the angular intensity variation.

A light meter built into the synchrotron responded to the visible spectrum radiated by the electrons and gave an indication of the average magnitude of the circulating electron current and served as a rough guide in controlling exposures. Because of the presence of fluctuations in the readings of this type of monitor, the exposures were actually recorded in terms of the readings of an ion current integrating meter[26] rather than in terms of the product of the light meter reading and the elapsed time. This integrating device served as a monitor of the synchrotron beam intensity in terms of the intensity of the bremsstrahlung produced when the accelerated electrons were allowed to strike a tungsten wire target. The beam of bremsstrahlung so produced fell on an ionization chamber with 1-in. copper walls. The ionization resulting from the electron showers produced in the walls of the chamber was used as a measure of the γ-ray intensity. For a given number of incident high-energy electrons the integrating meter reading is closely proportional to the electron energy, and for a given peak electron energy the reading may be regarded as proportional to the number of electrons acting as radiators. Hence the integrating meter readings gave an indication of the number of photons received by the photographic plate and could be relied upon as a measure of exposure.

By necessity the spectrograph was located in a region where the fast-neutron and gamma-ray levels were quite high. It was therefore necessary to ascertain to what extent the emulsion would be fogged by background radiation. Test plates were mounted in various positions within the spectrograph chamber. During comparable exposure times, no fogging was perceptible except in the case of plates located on top of the aluminum plate holder block with the emulsion side facing the metal. Plates similarly located with the emulsion side up were not affected. In another test, plates were mounted on the Rowland circle and the slit shutter was kept closed; otherwise the operating conditions were similar to those found in runs which had resulted in satisfactory registration of the spectrum. Upon development, the plates were found to be clear. It was therefore concluded that at least with the shutter closed, there were no harmful extraneous sources of radiation.

In order to exclude effects due to stray light and also to see whether the radiation did contain wavelengths in the far ultraviolet, metallic foils of Be and Al in turn were introduced into the path of the undispersed radiation. The foils were opaque to visible light but were sufficiently thin ($\sim$1000 A) to have a high transmission in the soft x-ray region, except in the immediate neighborhood of absorption discontinuities. The plates and microphotometer traces of the spectrograms taken with the two metal filters are reproduced in Fig. 13. As indicated in the diagram, the characteristic K and $L_{2,3}$ absorption edges of Be and Al, respectively, are clearly observable in two orders. From previous

[26] R. Littauer, Rev. Sci. Instr. 25, 148 (1954).

studies[27,28] it is known that the Be K edge is located at 111 A, while the $L_{2,3}$ discontinuity in the case of Al is at 170 A. The absorption spectra obtained in these exposures thus demonstrated that the radiation incident on the foils did extend into the 100 A region and that we were in fact dealing with the emission spectrum of radially accelerated high-energy electrons. These traces illustrate beautifully the usefulness of such a continuum in solid-state absorption spectroscopy. As far as known, these are the first absorption spectrograms obtained in the soft x-ray region using a continuum for the incident radiation.

In a subsequent run, two plates were positioned end to end so as to include the region of shorter wavelengths extending down to the central image. The resulting spectrogram and its microphotometer trace appear in Fig. 13(c). As before, this exposure shows little change in photographic density over the longer wavelengths. However, at the short-wavelength end near 60 A, there is a cutoff in intensity. This very rapid drop in intensity is now known to arise from the combined effects of the decrease in grating reflectivity and the actual termination of the incident spectrum.

The microphotometer traces in Fig. 13(d) were obtained by scanning in a direction at right angles to the Rowland circle at the wavelength positions indicated. Such traces were utilized in studying the angular spread of the radiation. To a casual observer, the traces shown in Figs. 13(c) and 13(d) do not present features which are exciting. It must be pointed out however that these traces are to be associated only with the photographic blackening which is a composite record of the spectrum of the source as modified by the dispersing instrument. The unraveling so as to arrive at the incident spectrum constitutes the major effort involved in these experiments.

In all exposures but one, the electrons were accelerated to the peak energy of the synchrotron (321 Mev). In one run however, the rf voltage was turned off early in the acceleration interval and in this case the maximum energy attained by the electrons was only 233 Mev.

The exposure was again governed by the integrating meter, making due allowance for the decrease in ionization current at the lower energy. Its indication was still assumed to be proportional to the peak electron energy.

The energies quoted throughout the text pertain to the peak energy at the stable orbit position and not as indicated by target radiation. As the rf voltage is turned off at the peak of the cycle when the magnetic field is nearly constant, the beam spirals into the target because of radiative losses and gives rise to the bremsstrahlung which the integrating meter detects. In this case the value of the energy indicated by the meter may be about 3 Mev less than that attained at the equilibrium orbit. When the rf is turned off earlier in the cycle, this difference will be even smaller. In this instance the increase in the magnetic field is also effective in causing the beam to move over and strike the target. Thus the energy at the stable orbit and that at the target are more nearly the same when the acceleration is stopped before reaching the peak of the cycle.

[27] R. W. Johnston and D. H. Tomboulian, Phys. Rev. 94, 1585 (1954).

[28] D. H. Tomboulian and E. M. Pell, Phys. Rev. 83, 1196 (1951).

II. Reduction Procedures

The reduction of a recorded spectrum must take into account factors which are characteristic of the source, the dispersing instrument, and the detector. Of necessity, several of these factors are different for widely separated regions of the spectrum. In order to point out the difference in the reduction procedures in the visible region as compared with those encountered in the vacuum region, considerations involved in the reduction of a near-ultraviolet spectrogram of the synchrotron continuum, such as the one shown in Fig. 12, will now be outlined. As stated previously, this was an exploratory plate obtained with a small quartz instrument not well adapted for quantitative work. Largely because of the excessively high photographic density attained for electron energies in excess of 70 Mev, most of the exposures were not suitable for quantitative treatment. However, one exposure, obtained at the relatively low electron energy of 60 Mev, appeared suitable for deducing the power spectrum.

The various diagrams included in Fig. 14 are intended to outline the steps involved in reducing such an exposure to obtain the spectral distribution of the source over this spectral region. From the microphotometer trace of the exposure one readily obtains

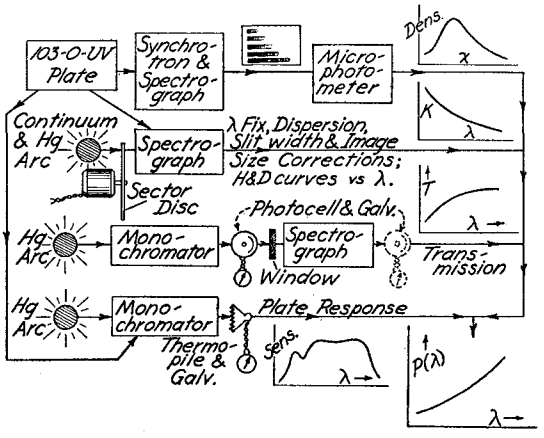

FIG. 14. Block diagram intended to illustrate the various steps involved in the reduction of a spectrogram obtained with a prismatic instrument in accordance with the procedures of heterochromatic photometry as discussed in the text. The relative spectral distribution curve shown in the lower right-hand corner is deduced from the photographic exposure by taking into account (1) the instrumental dispersion, image size variation, wavelength calibration, and transmission; and (2) the calibration and wavelength response of the emulsion.

the photographic density as a function of distance along the exposure. With this information as a starting point, the determination of the relative spectral energy distribution necessitates, on the instrumental side, a knowledge of the dispersion, wavelength calibration, and transmission of the spectrograph, and on the photometric side, the calibration and response of the emulsion.

The relation between the photographic density and exposure at various wavelengths was established in the usual manner by exposing a plate in the spectrograph to a mercury source. For each wavelength a step-sector disk placed in front of the slit was used to vary the exposure in a known way. (Exposures taken without the use of the disk served to determine the necessary correction to be applied for the change in image height with wavelength.) To intercompare the resulting *H-D* curves on an intensity basis, it was necessary to know what relative intensity at each wavelength gave rise to a prescribed value of the density, say 0.6. This was done by determining the relative intensities of a series of mercury lines with the aid of a thermopile placed in the focal plane of a grating monochromator. In this same plane, successive exposures to the same mercury lines were made directly on the photographic emulsion. In this step, a neutral filter (reduced aperture and rotating sector) was required to obtain accurate timing of exposures, which were adjusted to yield about the same density. No allowance was made for the photographic intermittency effect or the reciprocity law failure in any of the steps or for the fact that in the monochromator measurements, the radiation was incident normally on the emulsion, while in the spectrograph, considerably more oblique angles of incidence were involved. The wavelength response of the emulsion (Eastman type 103-0-uv) is sketched in a small plot in the lower portion of Fig. 14. The short-wavelength peak is due to the sensitizing lacquer and its wavelength position is in agreement with data published previously.[29]

The combined transmission of the vacuum-valve quartz window and the spectrograph was determined by using a 4-meter concave grating as a monochromator to simulate the narrow spread of illumination of the synchrotron exposure. Thus a beam of small angular divergence was allowed to pass through the system (with slit removed) along a path approximately that used in connection with the synchrotron exposure. Clearly, if the synchrotron radiation passes through a portion of the prism near its base, and on the other hand if the transmission of the system is measured with a beam traversing a section near the apex of the prism, an error will be introduced whose magnitude becomes larger as the absorption due to the quartz increases. For the transmission measurements, a 1P28 photomultiplier (with frosted envelope to avoid problems arising from point to point variation in cathode sensitivity) served to determine the incident and emergent intensity.

Ordinarily with a comparison spectrum placed alongside the unknown, the fixing of the wavelength scale presents no problems. Since no comparison spectra were superimposed on the exploratory plate, in fixing the wavelength scale recourse was made to the sharp photographic cutoff and low dispersion at the long-wavelength limit of the spectrum. Spectrograms of an incandescent source were made with the same slit width as that used in the synchrotron exposure. The resulting spectrograms were such as to approximate the steep rise in density observed in photographing the spectrum of the synchrotron continuum. Comparison mercury spectra, taken with a narrow slit, were superposed on the above spectrograms to establish the wavelength scale. Obviously, in more refined work, one would introduce a comparison spectrum on the synchrotron exposures directly.

The preceding discussion points out the many factors which enter into the reduction procedure to be followed in obtaining the actual source distribution. In the case of the 60-Mev run, the result is presented in Fig. 15

[29] Johnson, Watanabe, and Tousey, J. Opt. Soc. Am. **41**, 702 (1951).

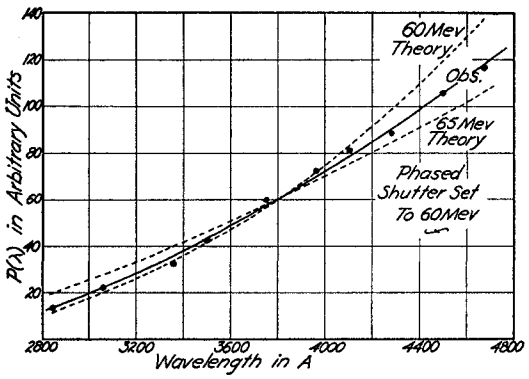

FIG. 15. Comparison of the reduced 60-Mev monoenergetic electron distribution with those calculated from theory at 60 Mev and 65 Mev. The ordinates have been matched at $\lambda = 3800$ A. Assuming the shutter setting to be correct, the experimental curve should agree more closely with the 65-Mev theoretical distribution, since, due to the width of the shutter opening, actually the the spectrograph can receive the radiation from electrons with energies up to 67 Mev.

along with the expected theoretical distribution at 60 Mev and 65 Mev. The experimental measurements represent the average of reductions based on two separate spectrograms. The results from the individual exposures were in good agreement, thus furnishing a check on the photometric procedure. For the sake of comparison, the experimental curve and those calculated from the formula [Eq. (5)] for the spectral distribution of monoenergetic electrons are matched at 3800 A. The agreement seems reasonable. Although the phase of the shutter was adjusted to admit the radiation from the 60-Mev electrons, actually due to the finite width of the shutter opening, the exposure received the radiation from electrons whose energies were spread over a 14-Mev band centered at 60 Mev. Therefore one would expect to find closer agreement with the 65-Mev rather than the 60-Mev theoretical curve.

When dealing with the problems of reducing plates obtained in the vacuum ultraviolet, one must again take into account similar factors characteristic of both the dispersing instrument and the detector. However, because of properties peculiar to the grating and photometric limitations encountered in this spectral region, there are significant and startling differences in making relative intensity measurements.

The various diagrams in Fig. 16 are intended to serve as an aid in describing the method of reduction of these plates. The problem as before is to extricate the source distribution function $P(\lambda)$ from the spectrographic record. To do this let us assume that the curve in Fig. 16(a) represents the average power spectrum emitted by a single electron whose energy is increased from zero to an upper limit sinusoidally with the time. A fraction of the power radiated by the electron will be incident on the grating. (For the present we shall be concerned only with the shape of the distribution curve and need not know the fraction of the emitted

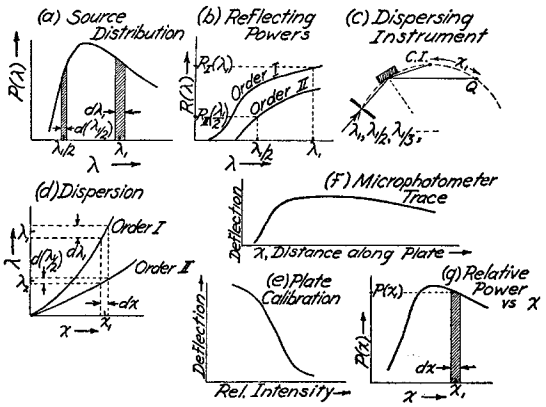

FIG. 16. Diagrams intended to illustrate the steps involved in the reduction of exposures obtained in the far ultraviolet by means of a grazing incidence spectrograph. Incident on the grating is the spectral distribution shown in (a). As in the ray diagram (c) the grating diffracts the radiation into various orders, so that at a given point Q in the focal plane, the energy collected per unit distance is due to radiation of wavelength λ_1 in the first order, $\lambda_1/2$ and $\lambda_1/3$ in the second and third orders. Also the incident intensity is modified by the grating according to the reflecting power curves given in (b). Experimentally one arrives at the relative power *vs* distance distribution curve in (g) from the microphotometer trace (f) of the exposure by using the plate calibration (e). The observed source distribution can then be determined by taking into account the instrumental dispersion curves of (d) and the reflecting power curves shown in (b). The important detail of the emulsion response is not considered.

power intercepted by the receiving device. This is governed by the geometry of the receiver and source.) The power incident on the grating over the narrow spectral band $d\lambda_1$, centered at λ_1, will be proportional to $P(\lambda_1)d\lambda_1$. A portion of this radiation will be scattered diffusely or absorbed by the grating. The remainder will be diffracted into various orders. At the given wavelength λ_1, the energy which appears in the first order is a fraction of the energy incident on the grating at the same wavelength λ_1. Let this fraction, i.e., the reflecting power of the grating, be denoted by $R_{\mathrm{I}}(\lambda_1)$. This quantity will vary with the wavelength in a manner which is characteristic of the material of the grating blank and groove shape. The wavelength dependence of the reflecting power for first and second order spectra is indicated qualitatively by the curves in Fig. 16(b). It follows that $R_{\mathrm{I}}(\lambda_1)P(\lambda_1)d\lambda_1$ is a measure of the power which falls into a vertical image of width dx, centered at x_1 on the Rowland circle. As shown in Fig. 16(c) the distance x_1 is measured along the circle from the central image C.I. to the point Q where the radiation of wavelength λ_1 is brought to a focus. In the absence of other contributions to the image centered at Q, we may write

$$P_{\mathrm{I}}(x_1)dx_1=P(\lambda_1)R_{\mathrm{I}}(\lambda_1)d\lambda_1, \tag{24}$$

where $P_{\mathrm{I}}(x_1)$ represents the power per unit distance interval at the position x_1.

In general, the incident radiation will contain shorter wavelengths $\lambda_1/2$, $\lambda_1/3$, $\cdots$. The radiation having these wavelengths will also be focused at Q in the second, third, or higher orders, respectively. Hence the fixed interval dx_1 at x_1 will also receive contributions corresponding to

$$P(\lambda_1/2)R_{\mathrm{II}}(\lambda_1/2)d(\lambda_1/2),\ P(\lambda_1/3)R_{\mathrm{III}}(\lambda_1/3)d(\lambda_1/3),\cdots$$

where $R_{\mathrm{II}}(\lambda_1/2)$ and $R_{\mathrm{III}}(\lambda_1/3)$ are the reflecting powers of the grating appropriate to the wavelength and spectral order. The wavelength intervals $d(\lambda_1/2)$, $d(\lambda_1/3)$, etc., must be chosen so as to correspond to the fixed distance interval dx_1, in accordance with the instrumental dispersion curves for different orders [see Fig. 16(d)]. In fact, it follows from the grating equation that the instrumental dispersion $d\lambda/dx$ at a fixed x varies inversely as the order, so that the wavelength interval $d(\lambda_1/2)$ is half as large as $d\lambda_1$ and $d(\lambda_1/3)$ is a third of $d\lambda_1$. Taking into account the contributions from higher orders, we can now write the more complete expression

$$P(x_1)dx_1=P(\lambda_1)R_{\mathrm{I}}(\lambda_1)d\lambda_1 +\tfrac{1}{2}P(\lambda_1/2)R_{\mathrm{II}}(\lambda_1/2)d\lambda_1+\cdots, \tag{25}$$

where $P(x_1)$ is the power per unit distance at x_1 due to the first- and higher order contributions.

In Eq. (25), only the first two orders have been considered, since over the wavelength range covered by the present measurements the third-order contributions are negligible. Dropping the subscript and solving for $P(\lambda)$, we obtain

$$P(\lambda)=P(x)\left(\frac{dx}{d\lambda}\right)\frac{1}{R_{\mathrm{I}}(\lambda)}-\tfrac{1}{2}P(\lambda/2)\frac{R_{\mathrm{II}}(\lambda/2)}{R_{\mathrm{I}}(\lambda)}-\cdots. \tag{26}$$

It follows that in determining the spectral distribution of the source we need to know: (1) $dx/d\lambda$, the reciprocal instrumental dispersion in the first order; (2) $R_{\mathrm{I}}(\lambda)$ and $R_{\mathrm{II}}(\lambda/2)$, the reflecting powers of the grating for the first- and second-order spectra; and (3) $P(x)$, the power per unit distance as recorded by the photographic emulsion. The values of $dx/d\lambda$ may be deduced from the wavelength *vs* distance curve in Fig. 16(d). The evaluation of $P(x)$ and the method used in determining the reflecting power will be discussed under separate headings.

In Eq. (26), the second term on the right is the contribution due to overlapping second-order radiation. Its magnitude presupposes a knowledge of the source distribution $P(\lambda)$. As shall be described presently, it turns out that $R_{\mathrm{II}}(\lambda/2)$ is zero for wavelengths shorter than a certain critical value, so that the portion of the observed spectrum which falls on the short-wavelength side of this critical value is free from second-order overlap. This fortunate circumstance makes it possible to obtain the $P(\lambda)$ *vs* λ curve directly by the use of Eq. (24) over the region where only first-order contributions are present. This segment of the curve is subsequently utilized to evaluate $P(\lambda/2)$ at the higher wavelengths where $R_{\mathrm{II}}(\lambda/2)$ is no longer negligible.

The distribution curve as formulated in Eq. (26) can then be constructed over the entire range by a piecemeal evaluation of portions free from overlap.

III. Photographic Photometry

In calibrating the photographic emulsion, one needs to correlate, at each wavelength, the incident energy (or the number of photons) per unit area of the emulsion with the photographic density resulting from the irradiation. Due to the nature of sources available in the vacuum region and the characteristics of spectrographs used, difficulties arise when attempting to vary exposures in a known way. One scheme is to compare the photographic densities of lines in spark spectra by varying the number of spark discharges in the exposure.

In calibrating the Q emulsion of the plates used in the soft x-ray region by this scheme, the source consisted of a condensed spark discharge in a glass capillary. Juxtaposed exposures of line spectra emitted by multiply ionized O, N, Si, Na, . . . atoms were utilized to construct the calibration curve. The scheme is based on the assumptions that: (1) at corresponding points of the images of a given line in spectra taken by varying the number of sparks, there is a constant ratio between the radiant energy received by unit area of emulsion; (2) in a given spectrum equal amounts of energy produce the same photographic density independently of the wavelength; and (3) intermittency defects and reciprocity law failures may be ignored. It is to be noted that assumption (2) presupposes one type of plate response "flatness." Another type might be that equal numbers of photons produce the same density independent of wavelength.

Suppose that one obtains two spectrograms of the same spark source, the exposure in the first being k times that of the second. In the microphotometer traces of the two exposures, now labeled as 1 and 2, the deflection d_A of a line A in trace 1 will be due to k times the radiant energy represented by line A in trace 2. Due to the richness of the spectrum one can almost always find a line B in trace 1 which has a deflection d_B equal to that of line A in trace 2. Let E_A represent the energy (in arbitrary units) which gives rise to d_A. Then the deflection d_B corresponds to an energy E_a/k. In a like manner, a series of deflections $d_A, d_B, d_C, \ldots$ may be correlated with the energies $E_A, E_A/k, E_A/k^2, \ldots$ and a calibration curve similar to the one sketched in Fig. 16(e) may be plotted.

Because of the lack of neutral detectors or sources of known intensity[30] distribution, the procedures of heterochromatic photometry cannot as yet be applied in the spectral region of interest. As already mentioned in the calibration process, we have been obliged to ignore the wavelength dependence of the emulsion energy sensitivity. We shall for the moment proceed on the assumption that the emulsion used in these measurements has this type of "flat" wavelength response in the 100 A to 300 A region. The alternative specification of "flatness" in terms of equal photon efficiency will be considered in connection with the discussion of the experimental results.

IV. Determination of $P(x)$

Due to the vertical angular spread of the radiation cone of each radiator, coupled with the fact that individual radiators are distributed in space, the total radiant power in a wavelength interval $d\lambda$ at λ, appears on the plate in a corresponding width dx at x but is spread over the height of the spectrogram.

In the case of a point source the situation may perhaps be visualized by referring to the sketch in Fig. 17 which again shows how, for a given radiation cone, the energy is collected only from orbital points lying between points a and b and how the radiation is dispersed by the grating (only first-order images are indicated). The diagram illustrates further how at any wavelength the image height is dependent both on the cone angle and on the distance from the source to the Rowland circle if small astigmatic effects at the grating are ignored. Focusing in the Rowland plane is not indicated.

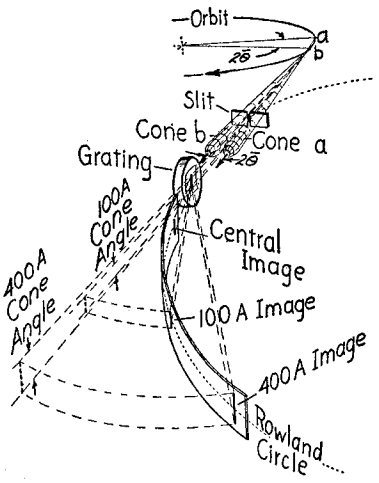

FIG. 17. Sketch depicting the manner in which the radiant power in a wavelength interval $d\lambda$ at a given λ is spread over the height of the spectrum. The diagram shows the radiation cones from two orbital points a and b. It illustrates how the image height, at each of two wavelengths ($\lambda = 100$ A and $\lambda = 400$ A), is dependent on the cone angle and on the distance from the source to the Rowland circle. Small astigmatic effects and focusing in the Rowland plane are ignored.

We must therefore measure a quantity proportional to the energy collected in an image of width dx extending crosswise to the spectrum whose vertical spread is not restricted by the aperture of the spectrograph. At a given λ, this quantity could then be correlated with the average power spectrum derived from an appropriate single electron distribution by summing over all cone angles, for the energies assumed during the acceleration interval and over the space distribution of electrons in the beam.

At a fixed position along the spectrum, say at $x = x_0$, a microphotometer trace taken crosswise to the exposure is shown by curve A in Fig. 18, while a plot of the corresponding intensity variation along the height of the spectrum is indicated by curve B. The ordinates in curve B were obtained from the microphotometer deflections with the aid of the calibration curve for the emulsion. The trace shown in curve A is typical and others taken at different values of x were similar in appearance. The sharply rising sides of the trace indicate that the instrument did not accept the entire vertical spread of the radiation. Indeed, all the traces

[30] The continuous radiation investigated in these experiments may in the future furnish a source whose spectral distribution may be regarded as known. For further comments see the concluding section of this article.

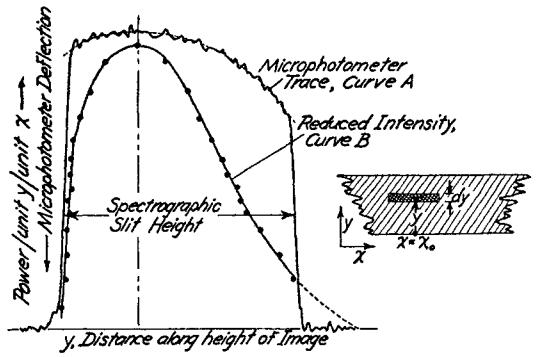

FIG. 18. The vertical intensity profile at a given wavelength position as derived from a crosswise tracing of the exposure. The steeply rising portions of the microphotometer trace in curve A indicate that the vertical spread of the spectrum was limited by the height of the spectrograph slit. The asymmetric appearance of curve B arises from the fact that the Rowland plane did not bisect the radiation cone accurately. If unrestricted by slit height, the area under curve B is proportional to the radiant energy received per unit length along the spectrum at the particular spectral position.

had the same width of 9.8 mm, which was very nearly identical with the actual height of the spectrograph slit. (The latter was located about 2.8 meters from the source of radiation.) Also the asymmetry of curve B points to the fact that the Rowland plane did not quite bisect the over-all radiation cone of the source, i.e., the Rowland plane was not the same as the orbital plane of the electron. A very slight inclination between the two planes was also indicated by a small vertical displacement in the trace of the position of the density maximum as function of distance along the plate.

In the diagram of Fig. 18 let dy be the effective scanning width of the microphotometer. In curve B let the ordinate, which represents the power per unit distance across and per unit length along the spectrum, be denoted by $P(x_0,y)$. Then the integral $\int P(x_0,y)dy$, taken over the unrestricted height of the spectrum, is proportional to $P(x_0)$, the power per unit length along the spectrum. Thus $P(x_0)$ can be measured in terms of the area under curve B (still not limited by slit height). Actually in obtaining $P(x_0)$, the intensity curve was assumed to be symmetrical and the desired area was evaluated by making use of the right half of curve B whose full extent was approximated by extrapolation.

An examination of a series of curves representing the cross intensity variation in the spectrum at different wavelengths leads to the observation that the actual areas under the curves are closely proportional (within 3%) to the maximum in the crosswise intensity variation. This is largely due to the fact that the various curves are quite similar in shape and have nearly identical widths when extended to cut the axis. This circumstance makes the intensity maximum a useful parameter in a more simplified scheme of reduction. In practice, it was therefore convenient to run the microphotometer trace along the spectrum at a height corresponding to the maximum in density. Deflections obtained in this manner could then be converted to intensities which gave the desired values of $P(x)$ within the approximation involved.

V. The Grating Response

As indicated by the formulation represented by Eq. (26), the reduction of the plates involves a knowledge of the energy distribution among the various order spectra produced by the particular grating as mounted for the purpose of these studies. A certain amount of information regarding the spectral response of the grating was already available previous to the undertaking which led to the determination of the reflecting power. This was based on the following observations derived from the examination of line spectra as well as the synchrotron continuum: (1) The radiation in the 60 A to 100 A range appeared only in the first order; (2) second- and third-order spectra were only observed for wavelengths higher than 100 A and 150 A, respectively. In addition, intensity ratios between the first- and higher order spectra were known with reasonable precision. The statements made under (1) and (2) may be verified by referring to the traces given in Figs. 13(a) and 13(c). For instance, in Fig. 13(c), the steep rise in intensity occurring at 60 A should have manifested itself in the second order, namely around 120 A. No sharp rise is observed in this vicinity. On the other hand, in Fig. 13(a) we see that the Be K edge located above 100 A is definitely present in the second order.

With this information as a background, an attempt was made to determine experimentally just what fraction of the energy incident on the grating was diffracted into the first and second orders. Such measurements necessitate the use of monochromatic radiations, so the grating response was measured at a few selected wavelengths by utilizing the sensibly monochromatic soft x-ray bands emitted by several light elemental solids. In particular, the K-emission bands of C and Be and also the $L_{2,3}$ spectrum of Al are suitably distributed over the wavelength range of interest. (The emission edges of C, Be, and Al bands are located respectively at 45 A, 110 A, and 170 A).

The techniques involved in the comparison of intensities will be found in another paper.[31] The results indicated that, at 110 A, 5.4% and 1.5% of the incident energy was diffracted into the first- and second-order spectra, respectively. At 170 A the corresponding quantities were 8.0% and 4.5%.

The solid part of the curves in Fig. 19 shows how R, the reflecting power, varies with wavelength from 40 to 188 A for the first- and second-order spectra produced by the grating used in the synchrotron investigation. The experimental values of R over this wavelength

[31] Sprague, Tomboulian, and Bedo, J. Opt. Soc. Am. 45, 756 (1955).

range as determined from various emission band data are predicted quite accurately by the plots. In harmony with the initial observations referred to earlier, the reflecting power curves show that (1) only first-order reflections are expected over the short-wavelength region, and (2) a marked increase in the intensity of second- and third- (not shown) order spectra sets in at successively longer wavelengths. In addition, over the region specified in Fig. 19, good agreement was found between the second-to-first order ratios predicted from these curves and those deduced from an examination of a large number of spectral lines.

Unfortunately, it was not possible to determine the grating response much beyond 200 A on the basis of measurements involving monochromatic radiations. Furthermore, the theoretical calculation of the reflecting power was not considered feasible in this region. Such a determination involves a knowledge of the wavelength dependence of the index of the grating blank. Over the spectral region extending up to 200 A the refractive index was calculated with the aid of dispersion theory on the assumption that all the L and M electrons present in SiO_2, taken as typical of the material of the grating blank, took part in the process. In view of the decrease in the energy of incident photons, in the region beyond 200 A, the above supposition regarding L and M electrons was no longer considered valid and no other independent scheme presented itself for arriving at the numerical value of the index.

However, in Fig. 19, the portions of the reflecting power curves shown by dashed lines beyond 200 A, constitute extensions based on synchrotron measurements. The manner in which these portions were deduced will be described in connection with the study of the average power spectrum obtained in the 233-Mev run.

E. RESULTS

The experimental results derived from the reduction of plates taken in the soft x-ray region will now be

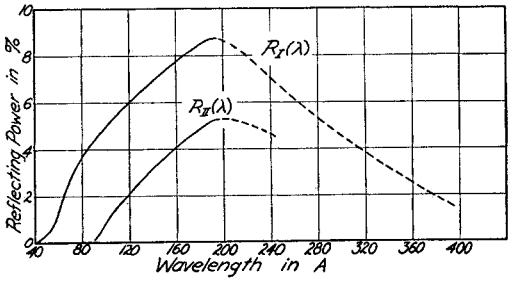

FIG. 19. The wavelength dependence of $R_N(\lambda)$, the reflecting power, for first- and second-order spectra of the grating used in the investigation of the radiation in the vacuum region. (The subscript N refers to the order.) The values of $R_N(\lambda)$ over the spectral range specified by the solid curves were derived from experimental measurements utilizing soft x-ray emission spectra of various solids. The values of $R_N(\lambda)$ beyond 200 A were determined from measurements based on the average power spectrum of the synchrotron radiation in the case of the 233-Mev run. Such values are represented by the dotted portions of the curves.

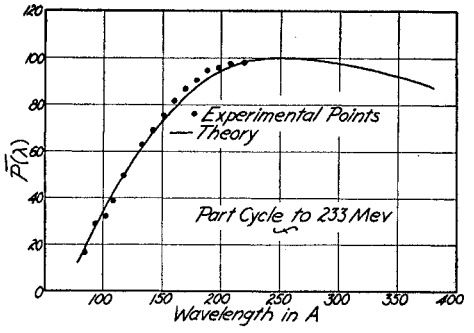

FIG. 20. The average power spectrum; part $\frac{1}{4}$-cycle acceleration interval. Over the 80 A to 200 A region, the experimentally observed distribution is indicated by circles. The distribution calculated from theory is shown by the solid curve. The observed values of $\bar{P}(\lambda)$ are matched at the peak of the theoretical curve. In this run the rf voltage was turned off when the electrons had acquired an energy of 233 Mev. Beyond 200 A, the experimental data were utilized to determine the reflecting power of the grating.

presented and compared with predictions from theory. The discussion will be divided into three headings and will include observations regarding (I) the shapes of average power spectral distribution curves, (II) the intensity variation with distance from center of image at given wavelength positions, and (III) the comparison of the energy radiated per angstrom using the measurements obtained from the 321-Mev and the 233-Mev runs.

I. Average Power Spectral Distributions

The information furnished by the grating response curves shown in Fig. 19 was first applied to the reduction of the 233-Mev trace. The calculations were carried out in accordance with the formulation of Eq. (26). The results as indicated by the circles in the plot of Fig. 20 outline the shape of the observed distribution over the spectral range extending from about 80 A to nearly 200 A. The data were normalized to an intensity of 100 at the peak. The wavelength interval is the one for which instrumental reflectivity curves were available on the basis of the calculations and tests carried out on the grating as cited previously. The measurements may be regarded as proportional to the energy per angstrom collected by the emulsion over the entire vertical spread of the spectrum and thus correspond to the average power per angstrom radiated by the electrons in the beam in all directions. It is therefore proper to compare the experimental observations with a plot of the function $\bar{P}_{\text{part}}(\lambda)$ representing the average power spectrum as predicted by the theoretical expression of Eq. (18). For the run in question, the rf voltage was turned off when the electron energy had reached the value of 233 Mev. Thus τ' defined by Eq. (20) and appearing as the lower limit of the integral of Eq. (19), here assumes the value $(321/233)^3=2.62$. A plot of $\bar{P}_{\text{part}}(\lambda)$ resulting from a numerical evaluation of Eq. (19) using this value of τ' was included in Fig. 5. The theoretical distribution with its maximum also

adjusted to a value of 100 is indicated by the solid curve in Fig. 20 and is reproduced for the sake of comparison with the observed experimental points.

An examination of the data presented in Fig. 20 reveals that over the range of short wavelengths a reasonably close correspondence is attained between the shape of the theoretical $\bar{P}_{\text{part}}(\lambda)$ curve and the experimentally evaluated relative intensity distribution. This aspect led us to believe that conditions at the source simulated the requirements of the theory and that the methods followed in the treatment of the data gave reliable results. Accordingly, in the long-wavelength region, the spectral distribution of the source was assumed to obey the theoretical relation. Still regarding the emulsion response to be flat on the energy basis, the experimental data available for wavelengths in excess of 200 A were therefore utilized to calculate the grating reflectivity. As pointed out previously, it had not been possible to obtain a reliable determination of the reflectivity in this spectral region by measurement or calculation.[32] The additional information concerning the grating response obtained on this basis is indicated in Fig. 19 by those dashed portions of the reflecting-power curves which lie beyond 200 A. Aided in part by this extension to the existing data on the grating efficiency, we proceeded to reduce the photometric measurements belonging to an entirely separate synchrotron exposure obtained from the run in which the electrons were accelerated during the full $\frac{1}{4}$ cycle to a peak energy of 321 Mev. The results of this reduction are again shown by circles in Fig. 21. The solid curve in this instance represents a plot of $\bar{P}_{\text{full}}(\lambda)$, the average power spectrum over a full cycle for $E_m=321$ Mev [see Eq. 15 and the plot in Fig. 5]. As before, the experimental points and the theoretical curve were normalized to 100 at the peak of the curve. It may be said that the experimental points reproduce the shape of the power distribution curve over a rather large spectral region, including that of the peak which is located at 85 A. (For $E_m=321$ Mev, $\lambda_m=169$ A as calculated from Eq. (14). Hence $\lambda_{\text{peak}}=0.50\lambda_m\cong 85$ A.)

At wavelengths close to the cutoff of the spectrum, the photometric reduction is subject to large errors. The corresponding microphotometer deflections are derived from the rapidly falling portion of the trace shown in Fig. 13(c). Also, over this region, the reflecting power varies rapidly with wavelength. These considerations can give rise to a large scatter in the result at the short wavelength limit of the spectrum. The experimental points represent the average of three reductions and a typical deviation of a single observation from the mean is indicated by vertical lines at three wavelengths in regions away from the cutoff.

It must be emphasized that in Fig. 21, the experimental observations in the region of the peak as well as those extending to about 200 A are determined independently of the synchrotron radiation, and are based on the grating response obtained with the aid of other soft x-ray sources. Beyond 200 A, the points are calculated by treating the corresponding region of the 233-Mev spectrum to be that of a standard source. The two sets of determinations are seen to join fairly smoothly and except at the longest wavelengths are distributed in the vicinity of the curve predicted by theory. Beyond 200 A, the contribution from overlapping second order radiation gets progressively larger. As can be seen from Eq. (26) the magnitude of this contribution is in part dependent on $R_{\text{II}}(\lambda/2)$ the second-order reflecting power and on the experimental values of $\bar{P}_{\text{full}}(\lambda)$ which are free from overlap. These two factors are evaluated independently of the 233-Mev run which has been utilized only to obtain the values of $R_{\text{I}}(\lambda)$. Thus, at wavelengths longer than 200 A, the shape of the 321-Mev experimental curve is considerably influenced by the shape of the same curve over the portion below 200 A. In the light of these considerations, there appears to be no inconsistency between the 321-Mev and the 233-Mev reductions.

The value of E_m used in these calculations is uncertain to within 1%. According to Corson,[33] the peak electron energy used in these experiments in all probability was

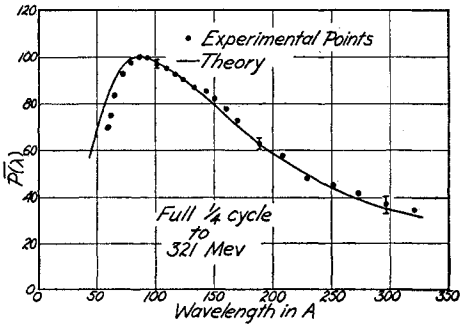

FIG. 21. The average power spectrum; full $\frac{1}{4}$-cycle acceleration interval. The experimental results extending from 60 A to 350 A are designated by circles. For the purpose of comparing shapes, the observed values of the relative spectral emittance are matched at the peak of the theoretically calculated distribution here shown by the solid curve. The electron energy varied sinusoidally with time and in this run the electrons attained the peak energy of 321 Mev.

[32] The values of the reflecting power obtained by this procedure were used to calculate the quantity δ, as defined by $\delta=1-n$, n being the refractive index. The values of δ can further be utilized to obtain a quantity which under the assumptions of normal dispersion theory, can be interpreted as the number of dispersion electrons per SiO_2 molecule, if one regards the composition of the grating blank to be similar to quartz. Excluding the K electrons, the molecule has twenty-four L and M electrons associated with the Si and O atoms and this number was used in calculating the reflecting power over the short-wavelength region. Over the longer wavelength range, the incident photon energies gradually get smaller and correspondingly the number of electrons per molecule participating in the dispersion act is reduced. The above calculations show that this number drops from 24 to about 4 over the wavelength range in question [see D. E. Bedo and D. H. Tomboulian, Phys. Rev. **99**, 624 (1955)]. The outcome of this calculation is quite reasonable and lends support to the above procedure adopted in determining the grating reflecting powers.

[33] D. R. Corson (private communication).

more accurately represented by 318 Mev. For this value of E_m, the peak intensity would fall at 88 A, rather than at 86 A. Indeed, the small change brought about in the shape of the $\bar{P}_{\text{full}}(\lambda)$ curve due to this reduction in the value of E_m is such as to improve the general agreement between theory and experiment. However, since the experimental errors are considerably larger than 1% it was not considered worth while to introduce this small alteration in the evaluation of integrals which had already been computed on the basis of $E_m=321$ Mev.

II. Intensity Variation with Height in Spectrum

As mentioned in connection with the method used in determining $P(x)$, it is possible to examine the intensity variation at right angles to the Rowland plane by obtaining a trace across the spectrogram (see again the plot in Fig. 18). The observed intensity variation is primarily due to the combined effects of the vertical spread of the radiation cone of each electron in the extended source, astigmatic effects being very small. In order to make some sort of comparison between the results of observation and those predicted from the angular distribution functions, it was assumed that the radiation was received from sources smeared uniformly over a circular section. Guided by our own visual observations on the source, we estimated the diameter of the beam cross section to be between 6 and 8 mm. For convenience in calculation it was taken as 6.8 mm.

Other observers estimate it as a smaller light source. Actually, no direct photographic measurements of the beam size appear to have been made. There are, however, two indirect measurements which have a bearing on the determination of the extent of the beam. These do not agree between themselves and are at variance with the somewhat *ad hoc* beam diameter assumed here. In the study of the activity (at the target of an expanded orbit) produced by the beam, Camac[34] finds a vertical spread of less than 2.5 mm and infers that the horizontal spread of the beam does not exceed 3.5 mm. Measurements by Corson,[33] based on the rate at which the beam sweeps over a target in the case of a contracting orbit, are consistent with a beam width of 12 mm. Both of these measurements were made on a "coasting" beam subsequent to the removal of the rf field—a circumstance which induces large vertical and horizontal oscillations. It is unlikely that either of these determinations will yield the width of the beam at the equilibrium orbit. The latter width is primarily what is seen in an optical observation which averages the extent of the source over a wide range of energies while the other measurements are made near the peak energy and are concerned with the extent, at the target position, in a beam subject to large oscillations. There is considerable latitude in the interpretation of the latter determinations. In fact, they may not be applicable

[34] M. Camac, Rev. Sci. Instr. 24, 290 (1953).

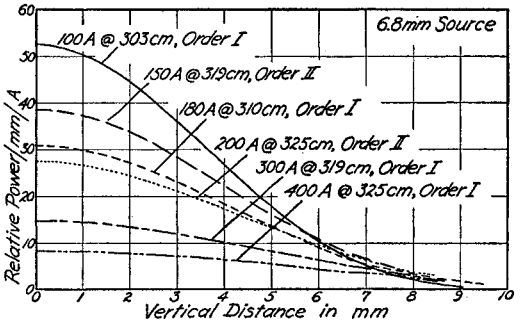

FIG. 22. The calculated intensity variation with height of spectral image for an extended source 6.8 mm in diameter. A given curve belonging to the family shows the vertical distribution at a particular position on the Rowland circle receiving radiation of the specified wavelength in the first or second order. The distance appearing in the label of a particular curve is the path length from the orbital point where the radiation originates, to the Rowland circle where the radiation is received. The vertical distances along the height of the spectrum are measured from the median plane. Only half of the actual spread is included in the plot. The calculations are based on the angular distribution curves of Fig. 8. In the above family of curves the ordinates representing the relative power per mm per A, do not include the modification in intensity introduced by the grating response.

to our situation. In any case, the arbitrariness regarding the nature and the size of our model must be recognized.

Now the radiation from the distant source is intercepted by the photographic plate at distances which gradually increase with wavelength. Hence, on the basis of the angular distributions presented in Fig. 8, the height of the image due to a *point* source can be determined at given wavelength positions since the source-to-plate distance is known from the experimental arrangement. In the case of the extended source postulated above, the resultant vertical spread[35] of the radiation may be obtained by an appropriate summation of point source intensity patterns at a fixed position on the plate. The curves reproduced in Fig. 22 represent superpositions of this nature. Neglecting the modification in intensity introduced by the grating response, the various plots in Fig. 22 depict the intensity variation with height at a particular position on the Rowland circle, due to the radiation of a given wavelength received at this position in the first or second order.

Over that region of the exposure which is free from second-order overlap, the predicted vertical intensity variation at a given wavelength position may be compared directly with the corresponding variation deduced from a crosswise tracing of the exposure. Comparisons of this kind are shown in Figs. 23(a) and 23(b) where the experimental determinations at various heights are indicated by circles. The data correspond to measurements carried out along the height of the exposure at 101 A and 179 A, respectively. The solid curves are

[35] Strictly speaking, owing to astigmatism the vertical distribution should also include a small additional spread in the individual point source patterns. This effect is essentially independent of position on the plate and is small so its influence upon the resultant distribution will be ignored.

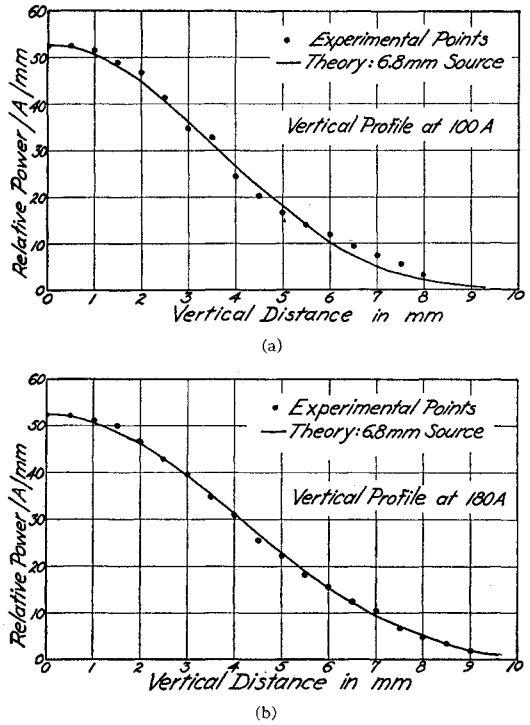

FIG. 23. Comparison between the predicted and observed vertical spread of the radiation at two wavelength positions in the spectral region free from order overlap. The experimental points shown in (a) and (b) are obtained respectively from measurements carried out along the height of the exposure at 101 A and 179 A. The solid curves represent the results of calculations carried out at 100 A and 180 A, respectively.

those found in Fig. 22 for $\lambda = 100$ A and $\lambda = 180$ A. The ordinates in the various plots are normalized so as to match at the peak. The shapes outlined by the experimental points agree surprisingly well with the results of calculations based on the adopted model.

Excepting the region near the short-wavelength limit, an examination of the shapes of a series of curves obtained at different positions throughout the exposure, indicates that the *observed* height of the spectrum changes but slightly. This observation can be explained by considering the overlap from second-order spectra and can be predicted on the basis of the information given in Fig. 22, by including the effect of the reflecting power of the grating for radiation occurring in the second order. As seen by referring to the values listed in Table I, the reflecting power for first-order radiation begins to decrease at wavelengths in excess of 200 A. Hence, relative to 180 A radiation, those at 300 A and 400 A suffer a considerable reduction in intensity. However, beyond 200 A, there is overlap due to short-wavelength radiation appearing in the second order. In this order, the reflecting power shows a considerable increase with wavelength. Hence the observed image height at positions corresponding to longer wavelengths is determined mainly by the vertical spread of the short-wavelength radiations which lie in the 100–200 A range and therefore possess heights comparable to those shown by the curves in Fig. 23.

To verify the foregoing statements with regard to the vertical distribution in the region of overlap, the expected intensity variation with height was calculated at two positions corresponding to $\lambda = 300$ A and 400 A in the first order. In so doing, use was made of the two lower curves in Fig. 22, to which second-order contributions were added after making suitable adjustments (for differences in dispersion and grating response) to the ordinates of the plot representing the spread of 150 A and 200 A radiations in the second order. The results are given by the solid curves in Figs. 24(a) and 24(b) for the two wavelength positions in question. The actual measurements of the crosswise intensity variations are again designated by circles. The agreement between observation and the composite curves including the effect of overlap is satisfactory. Thus, it may be concluded that the measurements on the height of the spectrum are not at variance with theoretical predictions. In fact, this aspect of the investigation is even more revealing than the corresponding study of the shape of the average power spectrum. Here one can see in a more detailed fashion just how the individual monochromatic angular distributions combine to account for the observed vertical characteristics of the spectrum.

It might be of interest to comment on the appearance of the spectrogram shape at the short wavelength limit. Here there is a rapid drop in the spectral intensity as well as in reflecting power. Accordingly, the height of the spectrum registered by the emulsion diminishes since, for a given exposure time, only the contribution coming from a narrowing spread near the peak of the distribution curves gives rise to a detectable blackening of the emulsion. (See again the intensity plot of Fig. 18.) This effect is seen in the 321-Mev spectrum reproduced in Fig. 13(c) where the exposure has a tapering appearance near the termination of the spectrum.

Admittedly the model adopted for the actual source may be somewhat artificial. However, as we have seen, it effectively predicts the observed width and the intensity variation in a direction normal to that of the dispersion. A reduction in the diameter of the smeared source or the assumption of a higher concentration of radiators over the central portion of the beam cross-section height would have resulted in narrower angular distributions approaching those for the limiting case of

TABLE I. Reflecting powers at various wavelengths for first- and second-order radiations. The values are expressed as percentages.

λ in A	$R_I(\lambda)$	$R_{II}(\lambda/2)$
100	4.8	0.0
200	8.7	0.9
300	4.5	3.6
400	1.3	5.6

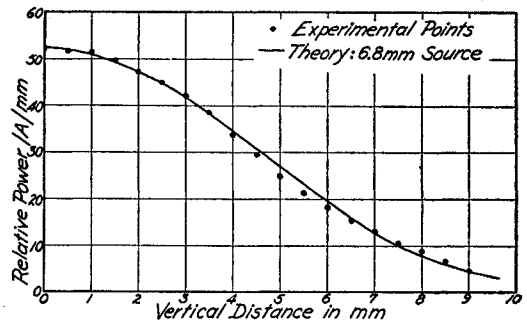

(a)

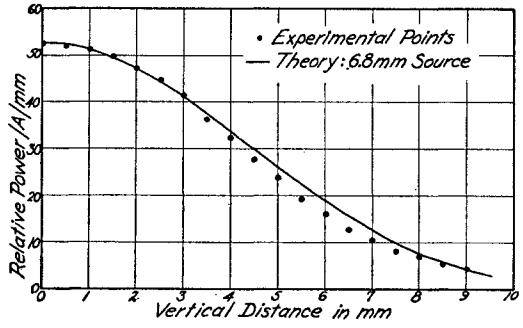

(b)

FIG. 24. The vertical distribution in the spectral region where there is overlap due to short wavelength radiation appearing in the second order. The solid curves in (a) and in (b) show the expected intensity variation with height at two spectral positions corresponding respectively to $\lambda = 300$ A and 400 A in the first order. The calculations take into account the contributions due to second-order spectra, suitable adjustment having been made for differences in dispersion and reflecting power. The experimental measurements were obtained from a crosswise tracing of the exposure at the two wavelength positions in question.

a point source, which would have yielded a spectrum roughly two-thirds as wide as that observed.

III. Comparison of the Energy Per Angstrom—Part and Full $\frac{1}{4}$-Cycle Runs

In addition to the consideration of the shapes of the spectral and angular distributions discussed in parts I and II, it is instructive to compare the energy per angstrom radiated at various wavelengths by making use of the measurements derived from the 321-Mev (full interval) and the 233-Mev (part interval) runs. Such a comparison utilizes additional information furnished by the readings of the integrating meter used in making the exposures.

At x_1, a fixed position on the microphotometer trace, $P(x_1)$, when corrected for second-order overlap, is a measure of W, the energy per unit wavelength band incident on the emulsion. For each of the two runs this energy is due to a certain number of electrons which took part in the emission process during the particular exposure. Although the absolute number of these electrons is not known, an estimate of the ratio of the number of electrons participating in the two different runs may be obtained in the following manner:

For a given number of electrons incident on the target used for monitoring the beam intensity, n, the number of "sweeps" recorded by the integrating meter is proportional to E, the electron energy at the target, i.e., $n = \text{const} \times E$. Assuming that the energy at the target is not very different from the maximum electron energy, the required sweep ratio should be $n_{321}/n_{233} = 321/233 = 1.38$ for the peak energies of 321 Mev and 233 Mev. In the present experiments 182 sweeps were recorded for the 321-Mev run. Hence, for an equal number of electrons falling on the target, the corresponding reading of the meter at 233 Mev should have been 182/1.38 or 132 sweeps. However, the actual exposure involved 240 sweeps in the case of the 233-Mev run, so that relative to the 321-Mev exposure, in this run, 240/132 or 1.82 times as many radiators participated.

From the expressions for the average power spectrum given by Eqs. (15) and (18), the energy per angstrom radiated by a single electron can be found by multiplying the expression for the average power by T and T' for the full- and part-interval accelerations, respectively. For the two exposures the ratio of two such energies at a specified wavelength λ, is found to be

$$W_{321}(\lambda)/W_{233}(\lambda) = 3[x^4 G(x)]/[x^3 I(x)], \qquad (27)$$

where the universal functions are to be evaluated at the particular value of x associated with the chosen λ through the relation $x = \lambda_m/\lambda$. Experimentally, the same ratio may be determined by comparing the value of $P(x)$, the energy per unit distance, as obtained from the two photometric reductions at a fixed distance x along the trace. [The latter quantity should not be confused with the parameter x in Eq. (27).] In so doing the second-order contribution must be removed and the observed ratio $P_{321}(x)/P_{233}(x)$ must be multiplied by 1.82 in order to take into account the difference in the number of radiators involved.

In Table II, the experimentally determined quantity $1.82P_{321}(x)/P_{233}(x)$ is listed for a series of wavelengths. To minimize photometric errors, the wavelengths were chosen only over the region (common to both traces) where the microphotometer deflections were relatively large (the density on the 233-Mev run was rather lower than what we would have preferred) and where the second-order corrections did not constitute a major

TABLE II. A comparison of the energy per angstrom emitted at a given wavelength by an electron accelerated, respectively, to peak energy of 321 Mev and 233 Mev.

λ in A	$1.82P_{321}(x)/P_{233}(x)$	$W_{321}(\lambda)/W_{233}(\lambda)$	Ratio
169	37.0	31.4	1.18
179	32.5	28.3	1.15
188	29.8	25.6	1.16
208	23.8	21.5	1.11
229	20.6	18.3	1.13
251	18.3	16.1	1.14
		Average	1.14

portion of the observed photographic density. The theoretical energy ratios were deduced from the appropriate plots of the functions appearing on the right-hand side of Eq. (27). The last column in the table shows the ratio between the evaluations based on the experimental curve and those calculated from the theoretical spectral distribution. The six determinations of this ratio, over a wavelength range covering 80 A, are scattered about the average value of 1.14. It may well be that the systematically high value of the ratio originates from the uncertainty in the value used for the relative number of radiators involved in the two experimental runs. It is estimated that this number (1.82) can be relied upon to within 5%.

F. MISCELLANEOUS COMMENTS AND CONCLUSIONS

I. Alternate View Regarding the "Flatness" of the Emulsion Response

As already described, for the lack of a better approach, the reduction of the spectrograms was carried out under the assumption that the emulsion possessed a flat response on the energy basis. More specifically, the implication is that equal amounts of energy at two different wavelengths give rise to the same photographic density. While plausible arguments may be given to support the assumption, the physical reasons underlying it are not proven. It was therefore considered worth while to investigate the influence of an alternate view regarding the nature of the emulsion response, namely that, as for x-rays, equal numbers of photons of different wavelengths produce the same blackening. Recalling the method described in obtaining the plate calibration curve by the use of spark spectra, it is seen that on the above assumption the quantity plotted as the abscissa in the calibration curve of Fig. 16(e) could just as well be taken to represent the number of photons per unit area as to represent the energy per unit area. With this understanding, $P(x)$, the experimental relative intensity is measured in terms of the number of photons per unit distance along the plate and must be expressed in energy units by taking into account the variation of the photon energy with wavelength. Following this conversion, comparison can again be made with the theoretical power spectrum curve.

Accordingly, the measurements were rereduced in the case of the 321-Mev run on the supposition that equal number of photons of different energy produced the same photographic blackening. This also involved determining a new grating response for the region beyond 180 A with the 233-Mev run, as before. The distribution curve derived on this basis is shown in Fig. 25 along with the corresponding theoretical plot of $\bar{P}_{\text{full}}(\lambda)$. It is plain that the alternate view leads to a large departure in the shape of the two curves. Also, in the long-wavelength region the experimental curve now shows a rising trend which is most unlikely. It might be mentioned that the values of the reflecting

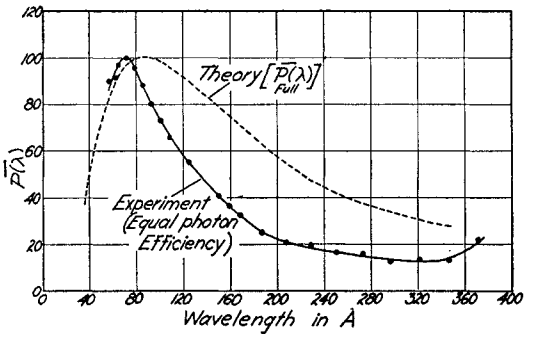

FIG. 25. A plot which illustrates the alteration brought about in the shape of the observed average power spectrum curve when an alternate view is adopted regarding the "flatness" of the emulsion response. If the exposure obtained in the 321-Mev run is reduced on the assumption that equal number of photons of different wavelengths produce the same blackening, the outcome is represented by the solid curve, determined by the experimental points indicated. The dotted curve portrays the shape predicted by theory. The same spectrogram when reduced on the basis of equal energy efficiency gives the result already presented in Fig. 21. It is clear that the procedure which supposes that the response is flat in energy yields a curve whose shape is in much better agreement with the theoretical plot of the energy distribution.

power which result from this modified treatment of the 233-Mev run are very low and lead to unreasonable values for the refractive index.

These discrepancies lead one to believe that the previous assumption with regard to the emulsion response is more reliable. In any event, the reduction procedure which supposes that the response is flat in energy, yields a distribution curve whose shape compares favorably with theoretical plots of the *energy* distribution and results in sensible values for the reflecting power.

II. Effect of Astigmatism

Since the grooves of the concave grating are ruled on a concave mirror as the blank, the images of spectral lines are, in general, astigmatic. The image of a point source located at the slit and radiating in all directions appears as a line whose length is given by[36]

$$l(\sin^2\alpha+\sin^2\beta\ \cos\beta/\cos\alpha),$$

where α and β are the angles of incidence and diffraction, respectively, and l is the length of the ruling. It follows that the effect is particularly large near grazing incidence where α and β are close to 90° and $\beta<\alpha$. If one takes all points of the slit into account, the image formed by the grating may be regarded as a series of of overlapping astigmatic images of slit points. In a conventional setup where an extended source is placed close to the slit, the rays originating from various points of the source are considerably inclined to the Rowland plane and the full height of the grating may be illuminated. This results in line images of large vertical extent.

[36] See for example, H. G. Beutler, J. Opt. Soc. Am. **35**, 311 (1945).

However, the circumstances in the present experiment are quite different. Here a small source, taken to be about 7 mm in extent, is located at a relatively great distance from the slit (about 3 m). What is more important is the fact that the rays have the very small vertical divergence of only about 3×10^{-3} radian. Thus they are essentially parallel to the Rowland plane and the effective length of the grating ruling is short. Using formulas given by Beutler,[36] one can calculate the height of the image due to a distant point source such as the electron at the orbit. Considering also the spread of the electrons in the beam, the results indicate that the astigmatic height of the image is only slightly greater than that expected on the basis of the angular width of the radiation cone. Furthermore, the image height is nearly independent of wavelength.

This expectation was confirmed in the negatives taken with the synchrotron continuum. If limited by the opening in the plate holder, the height of the emulsion which could have been exposed would have been twice the slit height. Yet the blackening did not extend to the edges of the plate holder. Over the entire spectrum the exposed region had sharp boundaries and very nearly a constant height equal to that of the slit (9.8 mm).

III. Energy Loss Due to Reflection at Surface of Emulsion

In connection with the plate response in the far ultraviolet, the assumed "flatness" presupposes that the fraction of the incident energy lost due to reflection at the surface of the emulsion is independent of the wavelength, that is, of the angle at which the radiation falls on the plate. Strictly speaking, this is not a valid assumption, but the variation in the fractional reflected energy should not be large over the limited range of angles (7°–15° from the surface of the emulsion) encountered in this work. On the other hand, the measurements of the grating reflectivity were carried out with the photographic plates positioned normally to the incident or diffracted radiation and should be essentially free of this difficulty.

IV. Attenuation of the Beam

In comparing the experimental curves with those based on theory, no allowance has been made for the possibility that the number of electrons participating in the radiation process at the end of an acceleration interval may be smaller than the number present at an earlier stage in the cycle. It has been assumed that there was no serious attenuation in the number of radiators in the beam after the electrons had attained an energy of a few tens of Mev.

V. Radiation Received while Electrons Spiral into the Target

In the experimental measurements dealing either with the angular or the spectral distribution, no correction has been made for the radiation received from electrons which spiral into the target after the rf voltage is turned off at the peak value of the magnetic field. The fact that energy will be collected by the plate during this interval may be understood by referring to the diagram in Fig. 9(b), and recalling that because of radiative losses the electron orbits will begin to shrink. The target is located at a radial distance of 39 inches which is 1 inch shorter than the mean orbital radius. Assuming that the magnetic field does not vary radially, this would correspond to a 2.5% or 8 Mev decrease from the peak energy of 321 Mev. However, because of the radial dependence of the magnetic field (see reference 17) the strength of the field increases slowly with diminishing orbital radius so that the actual change in energy is only 3 Mev. If one takes the radiative loss to be 900 ev per revolution [see Eq. (1)], this involves 3300 revolutions or a time of 66 μsec. Near the peak of the acceleration cycle the electron spends about 1200 μsec while its energy increases from 310 Mev to 321 Mev, so the energy collected during the contraction of the orbit amounts to about 6% of the energy collected over the 11-Mev range near the peak. Thus the additional radiant energy received while the electrons spiral into the target is small. This is a safe statement since the 6% figure ignores the energy collection over the earlier stages of the acceleration cycle. However, its effect upon the observed angular and spectral distributions must be recognized. Quantitatively the effect can be taken into account in the course of the numerical summation of the spectral and angular distributions at various energies by increasing the weighting factor of the monoenergetic 321-Mev distribution by about 6%. (Considerations of similar nature would be applicable to the case where the orbit is expanded by maintaining the rf voltage but allowing the field to decrease beyond the peak of the cycle.)

A further complication is involved in this correction. Referring again to Fig. 9(b), it can be seen that the radiation which is received from successively shrinking orbits, originates from orbital points having different azimuthal angles. The magnetic field may also be a function of this angle so that the orbital radius of curvature may have a complicated time dependence subsequent to the removal of the rf voltage.

VI. Applications

The electromagnetic radiation from centripetally accelerated high-energy electrons appears to be a useful by-product of such electron accelerators and is outstanding in its own right. Its continuous nature, high intensity, and wide spectral coverage are attractive features. Moreover, for a point source the spectral distribution is completely calculable, that is, the radiant energy can be expressed in absolute measure. These attributes lead one to believe that the continuum may serve as a standard in radiation measure-

ments both in the near and far ultraviolet of the spectrum as well as the visible.

Once the instrumental and procedural difficulties are surmounted, the source may be used to obtain the absolute calibration of various detecting devices utilizing counters, photoelectric surfaces, and photographic emulsions. Devices calibrated in this manner can be used as secondary standards by those who do not have access to the radiation itself.

In principle, one can calculate the average power per unit wavelength band (watts per angstrom) incident on a receiving area which accepts the full angular spread of the radiation. As outlined previously, this involves a knowledge of the relevant spectral distribution for a point source, the fraction of the radiant energy received by the spectrograph, and the dispersion and efficiency of the instrument. For an actual source, one must also know the effective number of radiators which contribute to the energy collected. In absolute calibration work this presents something of an obstacle. An appealing scheme to obviate it is to monitor a well-defined spectral region in the visible portion simultaneously with the exposure in the far ultraviolet. The measurement of the energy over the visible portion may be carried out by available calibrated neutral detectors. From this sampling of the radiation the effective number of radiators may be calculated by comparing the measured energy with that predicted from a single source distribution over the chosen limits of the spectrum in the visible.

Another application is in the use of the source for absorption studies in solid-state spectroscopy. Reference has already been made to sample absorption spectra obtained with the aid of the continuum. To deduce the shape of the absorption curve it is necessary to follow a reduction procedure which resembles the one followed in determining the shape of the average power spectrum. However, in this case the radiation incident on the slit is modified by the absorber placed between the slit and the grating. The effect due to an absorber of thickness t may be taken into account by introducing the factor $e^{-\mu(\lambda)t}$, where $\mu(\lambda)$ is the linear absorption coefficient. Imitating the steps used in formulating Eq. (26) and remembering that the absorption coefficient depends on the wavelength, we may write

$$P(x)\frac{dx}{d\lambda}=P(\lambda)e^{-\mu(\lambda)t}R_{\mathrm{I}}(\lambda)+\tfrac{1}{2}P(\lambda/2)e^{-\mu(\lambda/2)t}R_{\mathrm{II}}(\lambda/2)+\cdots, \quad (28)$$

whence

$$e^{-\mu(\lambda)t}=\frac{P(x)dx/d\lambda}{P(\lambda)R_{\mathrm{I}}(\lambda)}-\frac{1}{2}\frac{P(\lambda/2)e^{-\mu(\lambda/2)t}R_{\mathrm{II}}(\lambda/2)}{P(\lambda)R_{\mathrm{I}}(\lambda)}. \quad (29)$$

With the aid of Eq. (26) it is seen that, over the region where there is no second-order overlap, Eq. (29) reduces to

$$e^{-\mu(\lambda)t}=P(x)/P_0(x), \quad (30)$$

where $P(x)$ and $P_0(x)$ may be readily determined from exposures obtained with and without the absorber. The correction due to second-order overlap can be handled as before.

Absorption data for Be and Al obtained by the use of the synchrotron continuum have been reduced by following this procedure. The values of μ and the shapes of absorption curves so determined are in good agreement with similar but more laborious determinations obtained by exposing the absorber to the radiation from a spark discharge.

It is conceivable that the source may serve a useful purpose in problems involving the irradiation of biological specimens in the extreme ultraviolet. Or again, with suitable instrumentation designed to explore the region in the vicinity of the spectral maximum, the radiation itself could be utilized to determine the peak energy of electrons in the accelerator.

G. CONCLUDING REMARKS

The classical expressions describing the spectrum emitted by high-energy electrons moving in circular orbits have received experimental verification under a variety of circumstances. In the initial exploration by Elder, Langmuir, and Pollock,[11] radiometric measurements were carried out in the visible and near ultraviolet regions. These authors dealt with the average power spectrum emitted by electrons accelerated to peak energies ranging from 42.5 Mev to 80 Mev, in the small General Electric synchrotron whose orbital radius was 29 cm. As reported in the present paper, a rough check in the quartz region was made with the radiation from the old Cornell synchrotron (radius 100 cm) by the photographic registration of the spectrum over a small energy interval centered at 60 Mev. Of greater significance are the photometric studies of the average power spectrum in the vacuum region for the peak energies of 233 Mev and 321 Mev. The angular spread of the radiation was also examined at various wavelengths throughout the spectrum in the case of the 321-Mev run. With the aid of independent information regarding the relative number of radiators involved in the low- and high-energy runs, the energy per angstrom received at a given wavelength in the 321-Mev run was compared with the corresponding quantity in the 233-Mev run. The energy ratios obtained in this manner for a series of wavelengths were compared with the corresponding ratio deduced from theory. Perhaps one should also mention the side excursion which led to very acceptable values of the reflecting power by considering the radiation to possess the distribution ascribed to it by theory. In addition to these attempts designed to study the spectrum, there is Corson's work dealing with the measurement of the total radiative energy loss per revolution. Making due allowance for short comings in measurements, the

experimental evidence indicates in all respects satisfactory agreement with the classical theory of Schwinger.

ACKNOWLEDGMENTS

It is a pleasure to acknowledge the assistance received from various members of the staff of the Newman Laboratory of Nuclear Studies in the course of the experimental work with the synchrotron. In addition, the authors are obligated to Professor R. R. Wilson, the director of the Laboratory, for his interest in the experiments and for granting the use of facilities. They are especially grateful to Professors Corson, DeWire, and McDaniel for help received during the measurements and in subsequent discussions on matters pertaining to the accelerator.

Thanks are also due to Professor R. P. Feynman for illuminating comments on the theoretical aspects of the radiation and to Dr. G. Sprague and Mr. D. Bedo for valuable contributions to various phases of the work.

PHYSICAL REVIEW VOLUME 102, NUMBER 6 JUNE 15, 1956

Relationship between the Reciprocity Theorems of Onsager and of Callen-Greene*

THOMAS A. KAPLAN
Engineering Research Institute, The University of Michigan, Ann Arbor, Michigan
(Received February 9, 1956)

Onsager's reciprocity theorem is extended to linear non-Markoffian processes; the recipricity relation due to Callen-Greene is also extended to include the imaginary (as well as the real) part of the admittance matrix. In terms of these extensions, the two theorems are shown to be completely equivalent.

I. INTRODUCTION

THE Onsager reciprocity theorem[1] forms the basis of virtually the entire existing theory of irreversible processes.[2] More recently a "fluctuation-dissipation" theorem has been proved,[3] relating the equilibrium fluctuations to the dissipation parameter of an irreversible process. Extension[4] of the theorem to simultaneous processes again yields a form of reciprocity relation. This latter reciprocity theorem forms an apparent generalization of the Onsager theorem, as the symmetry is obtained for each Fourier component for general linear transient processes. The purpose of this paper is a critical examination of each of the reciprocity theorems so as to clarify their ranges of validity and their relationships to each other. It is shown that a reinterpretation of the Onsager theorem permits of its extension to linear non-Markoffian processes; that is, such an interpretation allows the kinetic coefficients to be considered as general functions of the time rather than as constants. Our examination of the fluctuation-dissipation theorem similarly leads to an extension of the reciprocity theorem derived therefrom: the imaginary part of the admittance matrix, as well as the real part, is shown to be symmetric. Finally, with the above described extensions of each of the reciprocity theorems, it is shown that both theorems have the same range of validity and are, in fact, completely equivalent.

* This work was performed at the University of Pennsylvania and supported by the Office of Naval Research. It is part of a thesis submitted to the Graduate School of the University of Pennsylvania in partial fulfillment of the requirements for the Ph.D. degree.

[1] L. Onsager, Phys. Rev. **37**, 405 (1931); **38**, 2265 (1931).

[2] S. R. DeGroot, *Thermodynamics of Irreversible Processes* (Interscience Publishers, Inc., New York, 1951).

[3] H. B. Callen and R. F. Greene, Phys. Rev. **86**, 702 (1952).

[4] H. B. Callen and R. F. Greene, Phys. Rev. **88**, 1387 (1952).

II. SUMMARY AND DISCUSSION OF THE TWO THEOREMS

A. Onsager's Theorem

Let us consider a closed system which may be described thermodynamically by a set of extensive variables x_i. For example we might have a closed system made up of two subsystems separated by a wall which permits the flow of heat and matter. Then the energy u and mole number n of one of the subsystems would constitute the set x_i. Equilibrium thermodynamics describes such a system in terms of the constrained equilibrium states accessible to the system. In the above example, a constrained equilibrium state would be one in which the differences in temperature and electrochemical potential between the two subsystems are nonzero, equilibrium being attained by replacing the diathermal, permeable wall by an adiabatic, impermeable wall. The unconstrained equilibrium state is the one for which the temperature and electrochemical potential differences are zero, this being reached physically if the diathermal, permeable wall is kept intact. Letting X_i be the values of the extensive variables in the unconstrained equilibrium state and a_i be the deviations $x_i - X_i$, we may define a set of "forces" γ_i in terms of the entropy function $S(\cdots x_i \cdots)$ (the total entropy of the closed system), by

$$\gamma_i \equiv \sum_k S_{ik} a_k, \tag{1}$$

where

$$S_{ik} = \partial^2 S(\cdots X_j \cdots)/\partial X_i \partial X_k. \tag{2}$$

Note that the γ_i as defined by Eq. (1) are approxi-

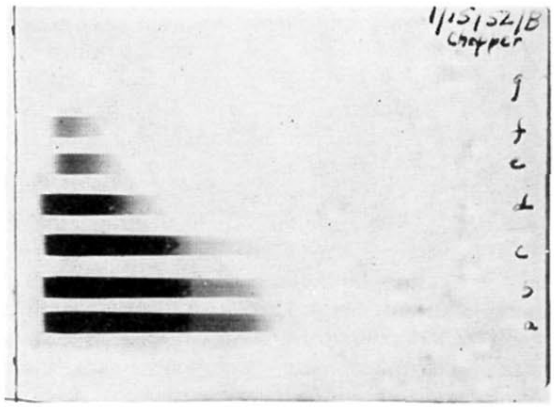

FIG. 12. Reproduction of a plate obtained with the arrangement of Fig. 11, showing spectra of the continuous radiation emitted by essentially monoenergetic electrons. The various exposures correspond to electron energies ranging from 60 Mev at the top to 110 Mev at the bottom. An exposure at 50 Mev is not visible in the reproduction. The exposures were adjusted so that, in each case, approximately the same total number of radiating electrons was involved.

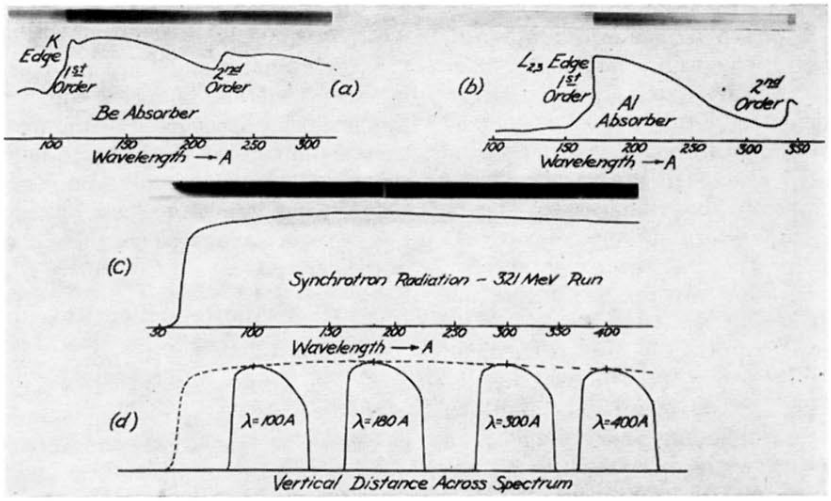

FIG. 13. Reproductions of the plates and microphotometer traces for three vacuum-ultraviolet spectra obtained by the use of the radiation from electrons whose energy was increased sinusoidally to a peak value of 321 Mev. (a) Radiation filtered through a thin Be film showing the K absorption edge which appears in the first and second order at 110 and 220 A, respectively. (b) Same radiation filtered through a thin Al film showing the $L_{2,3}$ edge in first and second order at 170 and 340 A, respectively. (c) The unfiltered synchrotron radiation. Due to the nature of the grating response and the presence of overlapping second-order radiation, the microphotometer trace of the exposure is surprisingly flat down to the abrupt cutoff at the short-wavelength region near 60 A. The tapered appearance in this region is related to the angular distribution. (d) Microphotometer records run crosswise to the exposure shown in (c) at four different wavelength positions. The traces show the angular intensity variation.